

Contents lists available at ScienceDirect

# Transportation Research Part A

journal homepage: www.elsevier.com/locate/tra



# LWR and shockwave analysis - Failures under a concave fundamental diagram and unexpected induced disturbances

Benjamin Coifman <sup>a,\*</sup>, Balaji Ponnu <sup>b</sup>, Paul El Asmar <sup>c</sup>

#### ARTICLE INFO

#### Keywords: Traffic flow theory Fundamental relationship Fundamental diagram Lighthill Whitham and Richards Loop detectors

Highway traffic

#### ABSTRACT

This paper undertakes a detailed empirical study of traffic dynamics on a freeway. The results show the traffic dynamics that systematically determine the shape of the fundamental diagram, FD, can also violate the stationarity assumptions of both shockwave analysis and Lighthill, Whitham and Richard's models, thereby inhibiting the applicability of these classical macroscopic traffic flow theories. The outcome is challenging because there is no way to identify the problem using only the macroscopic detector data. The research examines conditions local to vehicle detector stations to establish the FD while the single vehicle passage method is used to analyze the composition of vehicles underlying the aggregate samples. Then, traffic states are correlated between successive stations to measure the actual signal velocities and show they are inconsistent with the classical theories. This analysis also revealed that conditions in one lane can induce signals in another lane. Rather than exhibiting a single signal passing a given point in time and space, the induced and intrinsic signals are superimposed on one another in the given lane. We suspect the subtle dynamics revealed in this research have gone unnoticed because they are far below the resolution of conventional traffic monitoring. The findings could have implications to other traffic flow models that rely on the FD, so care should be taken to assess if a given model is potentially sensitive to the non-stationary dynamics presented herein.

The results have a direct impact on practice. Traffic flow theory is a critical input to many aspects of surface transportation, e.g., traffic management, traffic control, network design, vehicle routing, traveler information, and transportation planning all depend on models or simulation software that are based upon traffic flow theory. If the underlying traffic flow theory is flawed it puts the higher level applications at risk. So, the findings in this paper should lead to caution in accepting the predictions from traffic flow models and simulation software when the traffic exhibits a concave FD.

### 1. Introduction

The main argument of this paper is that certain traffic dynamics that systematically determine the shape of the fundamental diagram can also violate the assumptions of both shockwave analysis and Lighthill, Whitham and Richard's model, thereby inhibiting the

E-mail address: Coifman.1@OSU.edu (B. Coifman).

<sup>&</sup>lt;sup>a</sup> The Ohio State University, Joint Appointment with the Department of Civil, Environmental, and Geodetic Engineering, and the Department of Electrical and Computer Engineering, Hitchcock Hall 470, 2070 Neil Ave, Columbus, OH 43210, United States

b The Ohio State University, Transportation and Traffic Management, United States

<sup>&</sup>lt;sup>c</sup> The Ohio State University, Civil, Environmental, and Geodetic Engineering, United States

Corresponding author.

applicability of these classical macroscopic traffic flow theories. As will be discussed, the findings potentially impact other hydrodynamic models that rely on the same assumptions. The analysis to support the main argument also revealed that conditions in one lane can induce signals in another lane. Before getting to the arguments, a little background is necessary.

#### 1.1. Background

The scientific study of traffic flow is rooted in Greenshields's (1935) fundamental diagram, *FD*, that served as a building block for shockwave analysis used by Wardrop (1952) and its subsequent extension to hydrodynamic traffic flow models of Lighthill and Whitham (1955), and Richards (1956), denoted herein: *SwA* and *LWR*, respectively.

It is widely accepted that the FD is a static curve relating the three factors of the traffic state: speed, v, flow, q, and density, k. The shape of the FD curve can change over time and space (e.g., Munjal et al., 1971; Hall et al., 1992; Hsu and Banks, 1993; Van Wageningen-Kessels et al., 2010; Rudjanakanoknad, 2012, Duret et al., 2012, Wang et al., 2013; Srivastava and Geroliminis, 2013). Debate about the shape of the FD persists (e.g., Drake et al., 1967; Knoop and Daamen, 2017) in part because empirical traffic data are very noisy, thus, very different curves can fit a cloud of data points equally well. Traditionally, this noise is addressed by assuming stationary or "near-stationary" traffic states in the application of LWR (e.g., Breiman and Lawrence, 1973; Cassidy, 1998). The three-dimensional FD is usually expressed in terms of two dimensions with the third easily derived from the fundamental equation, q = kv. This paper will primarily focus on FD viewed in the flow-density plane, qkFD, since the qkFD is central to SwA and LWR. Two general shapes for the qkFD are common: "triangular," where the free flow regime and the congested regime are each captured with a linear relationship between q and k (e.g., Drake et al., 1967; Munjal et al., 1971, Hall et al., 1986; Newell, 2002), and "concave" shape where the free flow regime exhibits decreasing slope as q and k increase, then smoothly transitions after reaching capacity flow to the congested regime with q decreasing as k continues to increase (e.g., Greenshields, 1935). Hypothetical examples of triangular and concave FD are shown in Fig. 1. The early traffic flow theory literature almost exclusively considers concave qkFD, while evidence dating to the 1960's suggests that the triangular qkFD may arise from speed limits (e.g., Hall and Brilon, 1994; Hurdle et al., 1997; Bertini et al., 2006; Ponnu and Coifman, 2017). Regardless, it is clear that neither shape dominates all situations.

The SwA model states that the velocity, u, of the interface between any two states on the qkFD, A and B, is given by Equation (1). LWR extends SwA to hydrodynamic traffic flow models. The crux of the LWR model is that characteristic signals travel through the traffic stream to define the traffic state at all points in the time–space plane. The velocity of a given characteristic signal is given by the slope of the qkFD at the current traffic state; thus, the characteristic signals that define the traffic state propagate at velocity c given by Equation (2), where Q(k) denotes the functional form of the qkFD in terms of k.

$$u = \frac{q_A - q_B}{k_A - k_B} \tag{1}$$

$$c = \frac{dQ(k)}{dk} \tag{2}$$

#### 1.2. The argument

To date, conventional wisdom has led many to assume reproducibility of a qkFD equates to stationarity of the underlying traffic state. We hypothesize that the conditions that give rise to a concave shaped qkFD can also disrupt the dynamics necessary for LWR and SwA by violating the necessary assumption that the traffic state is, "sufficiently near stationary.".

LWR is predicated on the characteristic signals propagating slower than traffic, i.e., signals always propagate upstream in vehicle sequence. So a following driver must respond to their leader, and thus, provides a mechanism for the signals to propagate between vehicles. For example, Lighthill and Whitham (1955) state that their theory, "is applicable only to long, 'crowded' roads," where, "any increase in concentration will lead to a reduction in mean speed," and they clarify that although a wave may travel down the road, "the waves are always transmitted backwards relative to the vehicles on the road," i.e., signals will propagate upstream in vehicle sequence. Meanwhile, LWR includes the free flow regime of a concave qkFD, because c from Equation (2) is less than the traffic speed.

Some of the literature treats SwA as if it were synonymous with LWR, and that is an error. SwA predates LWR, e.g., as used in Wardrop (1952). Although under certain conditions LWR converges to SwA, e.g., in the propagation of shocks and the congested regime of a triangular qkFD, SwA is also divergent from LWR. SwA applies under a broader range of conditions because it is not a hydrodynamic traffic flow model and thus, does not depend on signals propagating upstream in vehicle sequence. For example, SwA still applies to the free flow regime of a triangular qkFD to capture signal propagation, but these conditions are outside the domain of LWR since in this case signals travel with the vehicles rather than the requisite propagation upstream in vehicle sequence.

Meanwhile, if SwA holds for a concave qkFD, when the state fluctuates between two points on the free flow regime of the concave qkFD, Equation (1) will yield a signal velocity u slower than the speed of either state, i.e.,  $u < v_A$  and  $u < v_B$ . Thus, like LWR, SwA applied to the free flow regime of a concave qkFD will predict signals should propagate over space at a velocity slower than the traffic speed.

<sup>&</sup>lt;sup>1</sup> Of course, other shapes of the qkFD curve remain in consideration by other researchers, the key feature for the present study is a concave shape in the free flow regime.

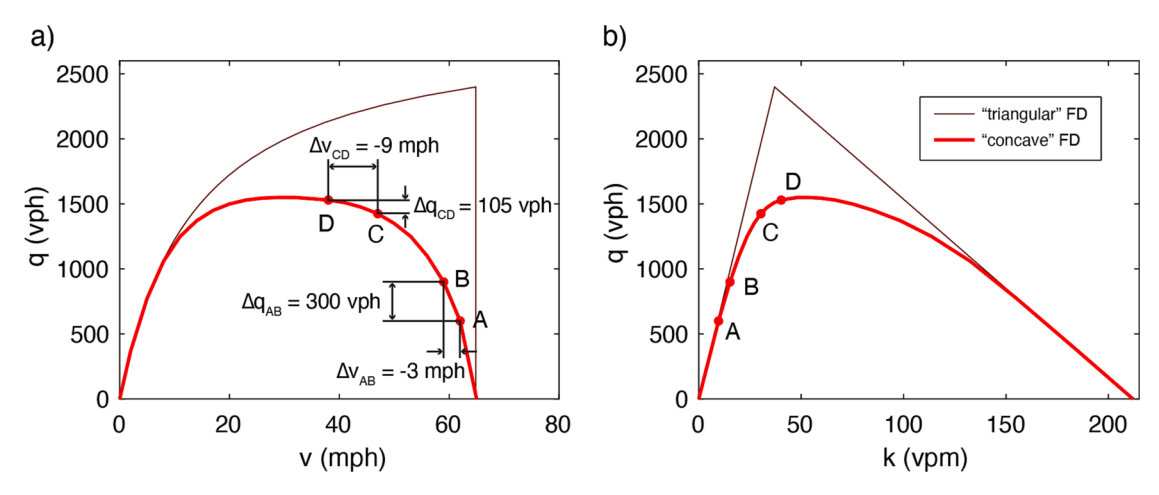


**Fig. 1.** A hypothetical triangular FD and concave FD, (a) in the speed flow plane (vqFD) with the axes transposed from conventional presentation to keep the q axis in line with, (b) the same FDs in the flow density plane (qkFD).

Instead of a stationary traffic composition, we postulate that the so-called free flow regime of a concave qkFD arises from a nonstationary mix of freely flowing vehicles who reach their desired speed before interacting with their respective leaders and drivers caught behind them who want to go faster. So a small number slower drivers exhibit truly free flowing dynamics and they become moving bottlenecks that trap many other vehicles in moving queues. The two groups of vehicles are distinct and behave very differently, with the resulting average traffic state falling between the state of the two separate groups and not being representative of either group taken individually. As a driver's preferred free speed drops, the greater the number of vehicles (on average) that will be trapped behind them, i.e., one should expect macroscopic q to be inversely proportionate to v and hence, the systematically reproducible concave shape to the emergent qkFD. In this context the emergent concave qkFD is a reproducible function of v that reflects the average number of vehicles that get caught in the moving queue behind a slow vehicle of the given speed, but reproducibility of the curve is different than stationarity of a given state on that curve. We hypothesize that: (1) the freely flowing vehicles do not respond to their leaders, violating Lighthill and Whitham's assumption that, "the waves are always transmitted backwards relative to the vehicles on the road." Instead, the void ahead of the slow moving vehicle serves as a buffer: as long as the slow moving vehicle is able to choose its speed independent of its leader, any signals moving upstream in vehicle sequence will terminate before propagating across the void. (2) The moving bottlenecks with the large void ahead and the pulse of demand in the moving queue behind will result in the traffic state propagating downstream with these vehicles. (3) The voids that form ahead of the moving bottlenecks pull the flow far below what could be sustained by homogeneous vehicles at the given speed. (4) For the reproducible concave shape to arise, the moving queues are relatively short- if a single slow moving vehicle amassed a large moving queue the state would fall strictly in the congested regime and the resulting macroscopic dynamics would be inconsistent with the free flow regime.

The general concept of moving bottlenecks is well established in the literature (e.g., Newell, 1998; Munoz and Daganzo, 2002, Leclercq et al., 2004; Logghe and Immers, 2008; Laval, 2009; Duret et al., 2010; Leclercq et al., 2016; Chen and Ahn, 2018). Each moving bottleneck should form a void of low flow ahead and high flow behind that moves downstream with the slow but truly freely flowing vehicle at the head of the queue. In this way, a slow vehicle that forms a moving bottleneck defines both the speed of the traffic and the velocity at which signals in flow propagate downstream (consistent with the observations of Edie and Baverez, 1967).

What is new is our supposition that when individual drivers exhibit a range of preferred free speeds, the duration for one of the voids to pass ahead of a slower driver can be much shorter than the sampling period of a vehicle detector, e.g., a void might last 10 s out of a 300 s sample. The non-stationary moving bottlenecks violate the assumptions of LWR and SwA, but because a typical conventional aggregated sample could contain several of these moving bottlenecks, it is impossible to detect their presence in the aggregated data. Meanwhile, the presence of the voids from several moving bottlenecks reduces the measured flow in the sample from what could be sustained at the given speed if the drivers had a more homogeneous preferred free speed.

In short, we postulate that the moving bottlenecks from the slower vehicles both violate stationarity and give rise to a concave shape in the free flow regime of the qkFD. As a result, long lasting signals should propagate downstream with the slower drivers rather than by LWR and SwA applied to the free flow regime of a concave qkFD, where LWR and SwA predict signals should propagate at a velocity slower than the traffic speed. The key word is long lasting, the assertion does not rule out signals that move upstream in vehicle sequence within the moving queues, but these upstream moving signals are short lasting because they should dissipate once they reach the void ahead of the next moving bottleneck.

This paper will also show that the stationarity violation is then exacerbated by lane change maneuvers. Lane change maneuvers have previously been shown to modulate the velocity at which signals travel, and on their own, they can violate the assumptions and applicability of LWR and SwA (e.g., Zhang, 2003). However, because we see the effect on links with high inflow, high outflow and close to zero in/outflow, the mechanism of lane changing modulating the signal velocity does not appear to be the dominant factor that violates the assumptions at the study site.

The key point of the present work is that the classical LWR and SwA models do not appear to hold in the free flow regime of a concave qkFD because the traffic dynamics that give rise to the concave qkFD also violate the assumptions of these classic models. To be clear, prior work has shown that these non-stationary dynamics arising from moving bottlenecks and lane change maneuvers could be accounted for with more sophisticated models (e.g., Zhang, 2002; Daganzo, 2002; Punzo and Tripodi, 2007; Yang et al., 2013; Qian et al., 2017). In other words, this work is focused on the fact that LWR and SwA do not apply in a situation where, by all conventional indications, these classical models seemingly should hold.

#### 1.3. Induced signals

Meanwhile, the tools used for this analysis also reveal previously unseen interlane dependencies and, in the process, provide empirical evidence to support an earlier hypothesis that anticipated their presence. Coifman and Ponnu (2020) demonstrated that the relative speed to adjacent lanes can systematically modulate the shape of the qkFD in the ego lane, and as a result, they hypothesized that the resulting change in the qkFD shape will also impact the velocity at which signals propagate over space. However, that work only considered the shape of the FD, it did not measure any actual signal propagation over space.

In light of these facts, we postulate that disturbances propagating in lane 2 can induce disturbances in lane 1 that travel with the signal in lane 2. Specifically, when the speed in lane 2,  $v_2$ , changes the findings of Ponnu and Coifman (2017) indicate that lane 1 should shift to a different FD curve. In other words,  $v_2$  should modulate which qkFD curve the traffic state in lane 1 falls on, as illustrated in Fig. 2b. The modulation in lane 1 due to a specific value of  $v_2$  propagating in lane 2 will travel with that disturbance in lane 2. As such, this dynamic qkFD provides a mechanism for induced signals. Since the dependency arises from local speeds, it should not be limited to a specific regime of operation<sup>2</sup>, however, when both lanes are operating in the same regime it would be difficult to separate the induced behavior from the intrinsic behavior of the given lane because both the induced and intrinsic dynamics will result in signals traveling the same direction. So any induced signals in lane 1 should be most apparent when lane 1 is free flowing and lane 2 is congested because the induced and intrinsic signals should travel in opposite directions.<sup>3</sup>

This interlane dependency leads to the following corollary: the induced signals should primarily impact v, with little or no measurable impact on q. Because the speed in lane 2 determines which FD curve lane 1 operates on, for the hypothetical example in Fig. 2b each of the three qkFD curves arise from different values of  $v_2$ . Since  $v_2$  can take any real value between 0 and free speed, there should be a continuum of qkFD curves in lane 1. As a signal in  $v_2$  passes a given location, each value of  $v_2$  pulls lane 1 to a different FD curve. This mechanism locks the response in lane 1 to the stimulus in lane 2. Conservation of vehicles in lane 1 dictates that the flow in lane 1,  $q_1$ , should not change in response to a local change in  $v_2$ . If  $q_1$  does not change, then these dynamics would ensure that the induced transitions in the flow-density plane for the impacted lane should be close to horizontal, with  $u \approx 0$  via Equation (1). In other words, at any given location the changes in lane 1 speed should amount to zero velocity waves via SwA, triggered by changes in the current speed in lane 2 at that location, superimposed on the downstream moving free flow traffic states in lane 1. While the intrinsic traffic state evolves along the qkFD, e.g., Fig. 2a, fluctuations in  $v_2$  should modulate the shape of the qkFD in lane 1 as illustrated in Fig. 2b. Since  $v_2$  propagates upstream in congested lane 2, the perturbed qkFD in free flowing lane 1 will also travel upstream with  $v_2$ , giving a secondary mechanism for signals and waves to propagate in the traffic stream. The combined influence of  $q_1$  and  $v_2$  are shown in Fig. 2c.

#### 1.4. Overview

The remainder of this paper is laid out as follows: Section 2 opens by laying out the data measurement techniques used in this work. The focus then moves to an empirical analysis of the composition and stationarity of traffic in the free flow regime of a concave qkFD from a high occupancy vehicle, *HOV*, lane as observed at various detector stations. Shifting to spatial factors, the empirical analysis examines the velocity at which the traffic state propagates over space by correlating time series traffic data between several pairs of successive detector stations. The paper closes in Section 3 with discussion and conclusions.

#### 2. Analysis

The work examines an HOV lane that can sustain a high relative speed to the adjacent general purpose, *GP*, lane. This paper uses the empirical data set from Ponnu and Coifman (2015), consisting of individual vehicle actuations at dual loop detectors. The data come from the Berkeley Highway Laboratory, *BHL*, (Coifman et al., 2000), a roughly 2 mile long stretch of eastbound I-80 in Emeryville and

<sup>&</sup>lt;sup>2</sup> For example, Coifman and Ponnu (2020) showed the interlane dependencies go both ways, with slower lanes exhibiting a dependency to conditions in adjacent faster lanes.

<sup>&</sup>lt;sup>3</sup> The same should be true for free flowing lane 1 inducing downstream moving signals in congested lane 2, but detecting the counter-flow signals is more challenging in this scenario. Coifman and Wang (2005) showed that in addition to the expected upstream moving signals in congestion, for an inhomogeneous vehicle fleet the congested traffic should also carry signals downstream with the vehicles as a result of the different vehicle lengths. These intrinsic downstream moving signals in a congested lane would confound the identification of induced downstream moving signals.

<sup>&</sup>lt;sup>4</sup> In practice we suspect that the modulating signals will not have a perfect u = 0, which should generate noise in the form of signals that travel through the traffic stream. Exploration of this suspicion is left to future work, for the sake of the current study it is assumed that their impacts are negligible.

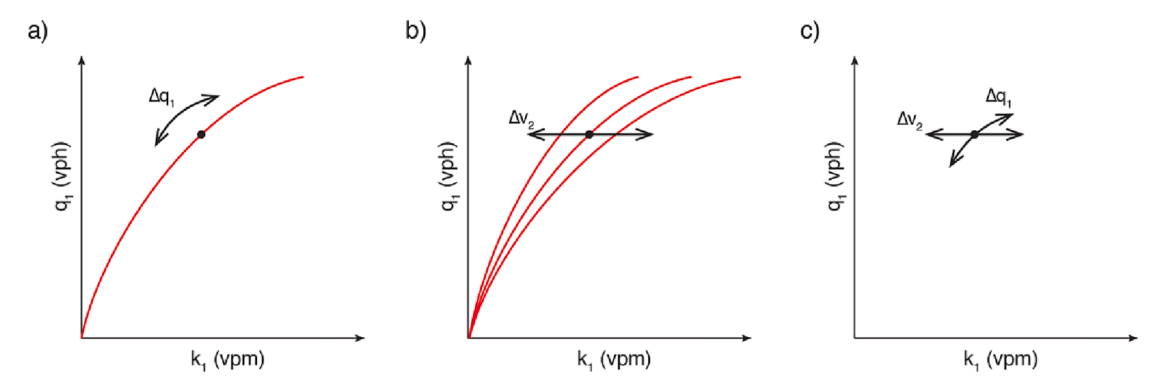


**Fig. 2.** (a) A hypothetical concave qkFD in the free flow regime showing how the traffic state is conventionally accepted to fluctuate along the FD curve as  $q_1$  changes. The slope of the tangent is positive and varies with  $q_1$ , thus, SwA dictates that signals will propagate downstream at different speeds. (b) Showing the same curve from part a among a family of qkFD curves, the exact curve where the traffic state falls is a function of  $v_2$ . In this case, the transition from one curve to another has a slope of zero as  $v_2$  varies, i.e., via SwA, the signal should not travel in space. So  $q_1$  should remain (roughly) constant as  $v_1$  and  $k_1$  respond to  $v_2$ . (c) A superposition of the two factors from parts a & b.

Berkeley, California. As shown in Fig. 3, the freeway has 5 lanes, numbered from the inside (median) lane 1, to the outside (shoulder) lane 5. Lane 1 is a time of day HOV lane that reverts to GP outside of the period of HOV operations. The only distinctions that drivers see of lane 1 are diamond markings on the pavement and signage along the right of way. The width of lane 1 and striping between lanes 1 and 2 are otherwise identical to that of the GP lanes. The data come from 70 weekdays in September through December in 1999 from dual loop detector stations 1–7 in the BHL, skipping station 5 due to a bad detector. The speed limit at the time of collection was 65 mph. This study uses two different time windows for the I-80 data around the evening peak period, the first time window is while the HOV restriction is active, termed "HOV period", between 15 and 19 h. The second time window is used for reference and comes from when lane 1 serves as a GP lane, termed "non-HOV period" during 13–14.75 and 19.25–21 h. Trucks are restricted from lanes 1 and 2, though somewhat frequent buses and an occasional violating truck can be seen in these lanes. The analysis will consider both lanes 1 and 2, so we employ a subscript 1 or 2 to denote the lane a given metric is from. Section 2.1 studies conditions as seen at the individual detector stations, while Section 2.2 looks at the propagation of signals between detector stations.

#### 2.1. The shape of things at detector Stations- understanding the composition of a concave qkFD

Traffic measurements typically come from point detectors, e.g., the dual loop detectors used in this study, and the data are usually aggregated over fixed time periods. Fig. 4 shows a scatter plot of the 5 min average flow versus occupancy in lane 1 at station 2 from 55 days during the HOV period and separately the non-HOV period. In both cases almost all of the 5 min samples appear to come from the free flow regime. Clearly, the same lane at the same detector station exhibits very different behavior depending on the time of day. Fig. 4a shows the flow-occupancy relationship in the HOV lane while the HOV restriction is active and the fact that speed drops with increasing flow is consistent with a concave qkFD. While Fig. 4b shows the results for the same lane when the HOV restriction is not active, i.e., the lane reverts to being a GP lane, and the fact that speed is nearly constant throughout the free flow regime is consistent with a triangular qkFD. So in principle, conditions during the HOV period should be compatible with LWR while conditions during the non-HOV period are not. The HOV and non-HOV periods are shown together in Fig. 4c.

The remainder of this section looks closer at the point measurements in lane 1 during the HOV period. Section 2.1.1 looks at the composition of the vehicles seen in lane 1 and their contribution to the aggregate traffic state, while Section 2.1.2 extends the analysis to explore impacts from the adjacent lane.

#### 2.1.1. The contribution of a single vehicle passage

To facilitate the discussion in the context of LWR, the flow-occupancy data in Fig. 4a are projected to the flow-density plain in Fig. 5a and a second order linear regression curve  $Q_1(k_1)$  has been fit to the data over the range of  $k_1$  from 10 to 40 vehicles per mile (vpm). The curve is shown with dashes beyond  $k_1 = 35vpm$  since the number of observations and the quality of the fit both drop off in this region. The fitted curve is shown without the underlying data in Fig. 5b. Although not shown, we repeated Fig. 5a-b for lane 1 at each station. As will be discussed later, the exact shape of the fitted curve varied from station to station, but always exhibited the general concave shape shown for station 2.

Now consider the constituent vehicles underlying the aggregate data during the HOV period in Fig. 5a. For each single vehicle passage, svp, the flow,  $q_{svp}$ , occupancy,  $occ_{svp}$ , speed,  $v_{svp}$ , and length,  $L_{svp}$ , are calculated via Equations 3–6 (Coifman, 2014b). Where

<sup>&</sup>lt;sup>5</sup> The remaining 15 days were excluded for clarity of presentation because lane 1 exhibited congested conditions that extended the point cloud into the congested regime. Rather than use an arbitrary threshold to exclude the congested observations the data set was large enough that for this figure we simply excluded the days with any congestion in lane 1.

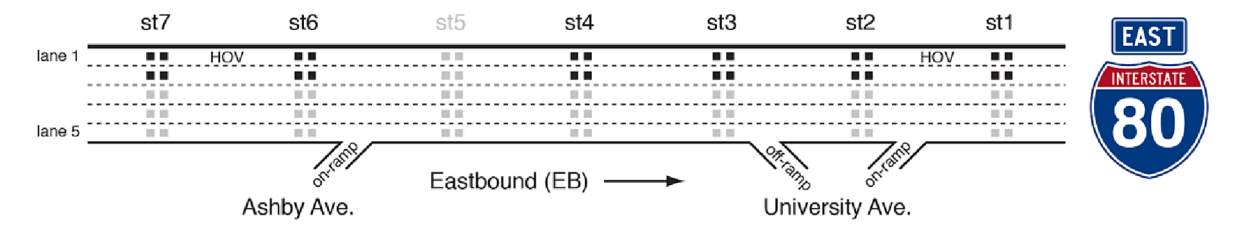


Fig. 3. The portion of BHL on I-80 in Berkeley, CA used in this study (not to scale), with squares denoting loop detector locations: black squares being those used in this study and gray not used. Station 5 was not used in this study because one of the loop detectors in lane 1 at this station was inoperable.

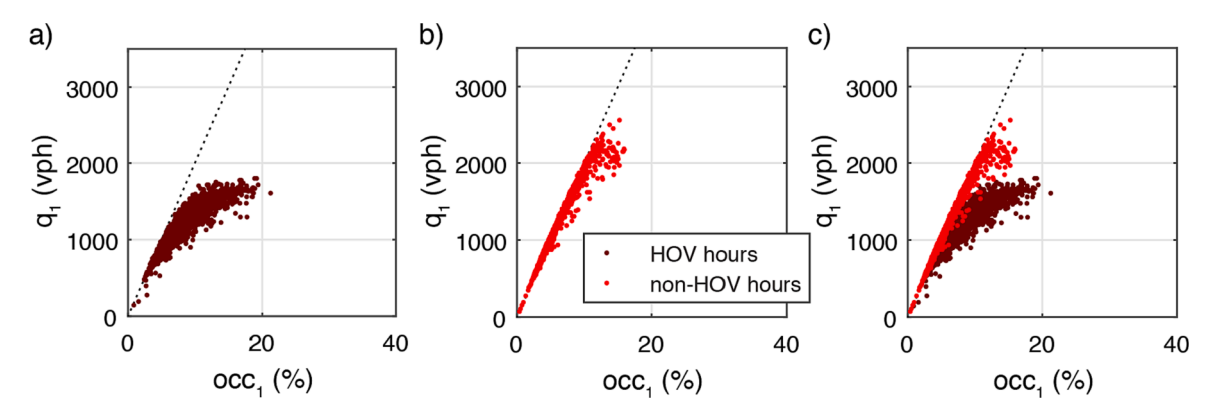


Fig. 4. The emergent qoccFD from 5 min average data from 55 typical weekdays in 1999 in lane 1 at station 2 for (a) the HOV period, 15–19 hr, (b) the non-HOV period, 13–14.75 hr & 19.25–21 hr, and (c) both together. Note that the dashed lines are simply for reference to facilitate comparison across plots.

h is the headway of the vehicle measured rear bumper of the previous vehicle to the rear bumper of the current vehicle to ensure that the gap ahead of the current vehicle is associated with that vehicle since ultimately a given driver controls the gap ahead of themself. On-time is the time for which the vehicle occupied the upstream detector, detector spacing is the distance between the leading edge of each loop of the dual loop detector. The traversal time is the difference between the actuation times at the downstream and upstream detectors. Taking the HOV period data in lane 1 from all 70 days and six stations, we bin the  $q_{svp}$  data by resolvable  $v_{svp}$ . and only retain passenger vehicles,  $18ft \le L_{svp} \le 22ft$ , to eliminate the impact of inhomogeneous vehicle lengths (Coifman, 2014a). This length range includes roughly 70 % of the vehicles seen in lane 1. For each bin we find the harmonic mean value of q, and then calculate k for that bin via the fundamental equation (Coifman, 2015). The resulting curve is shown with circles in Fig. 5c, where solid circles denote 70 > v > 45 mph, and open circles denote 45 > v > 30 mph. Although this plot uses more days and all stations, it clearly traces out a concave shaped qkFD for the HOV period, consistent with Fig. 5a-b but with less scatter since there are over 600,000 individual vehicle actuations underlying this curve, with several orders of magnitude more vehicles per point compared to Fig. 5a.

$$q_{svp} = \frac{1}{h} \tag{3}$$

$$occ_{svp} = \frac{on\_time}{h} *100\%$$
 (4)

$$v_{svp} = \frac{detector\_spacing}{traversal\_time} \tag{5}$$

$$L_{svp} = v_{svp} * on\_time$$
 (6)

At this point the most important factor is the concave shape of the qkFD. Whether binning by 5 min samples (Fig. 5a) or binning by length and speed (circles in Fig. 5c), the aggregate data exhibit a concave shape in the free flow regime of the qkFD. By most conventional assessments, given the clean concave qkFD, this lane should be well represented by the LWR and SwA models. But most conventional assessments assume that since the qkFD yields a tight band of reproducible states, that the underlying states should be sufficiently near stationary for the classical models to hold.

Consider the microscopic dynamics that can give rise to the macroscopic concave qkFD exhibited in Fig. 5a-b. If there is a distribution of preferred free speeds,  $v_{FP}$ , among drivers, and the only source of delay is a vehicle with a higher  $v_{FP}$  getting stuck behind another vehicle with a lower  $v_{FP}$ , then a vehicle with the lowest  $v_{FP}$  should always be able to achieve and maintain their  $v_{FP}$ . Thus, this

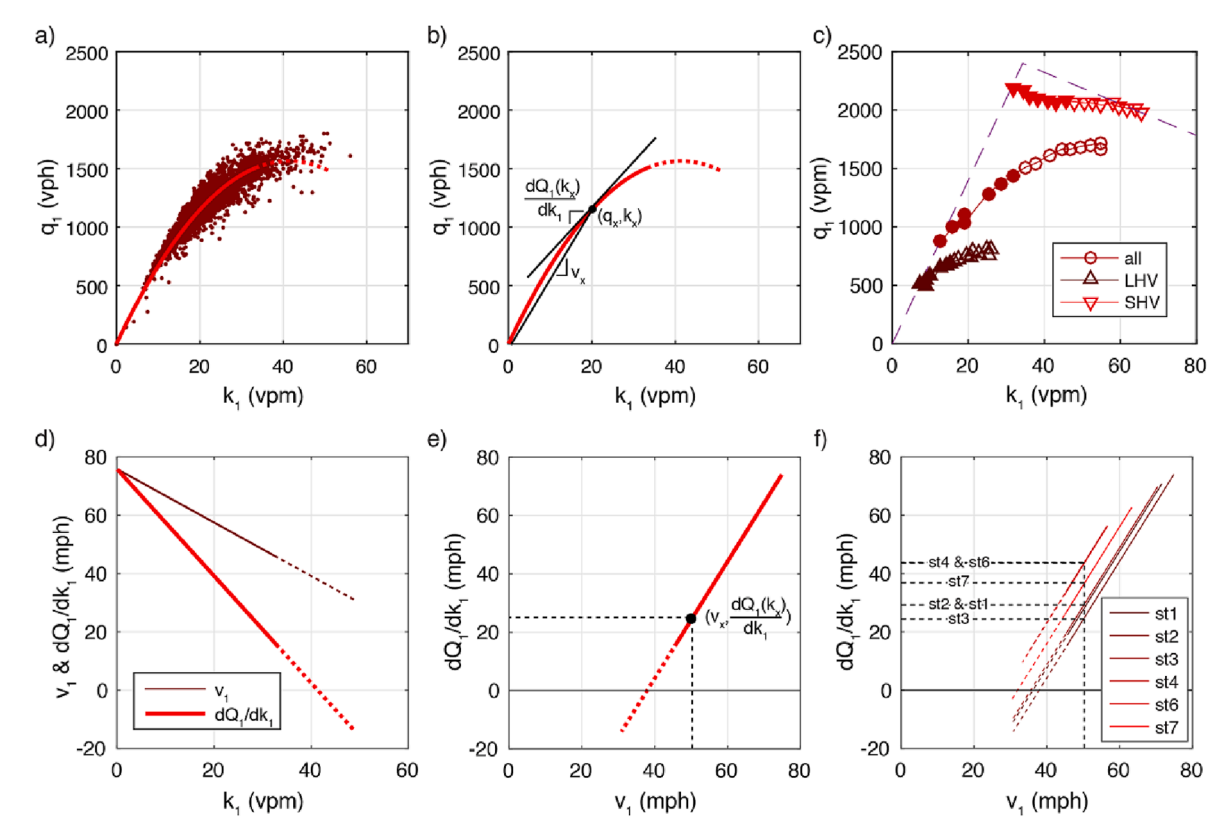


Fig. 5. (a) Fig. 4a projected in to the qkFD plane and fitted with a curve. (b) The fitted curve without the data to illustrate the relationships between key parameters. (c) Emergent qkFD curves from the svp method applied to all vehicles, LHV, and SHV (the dashed line is for reference to facilitate comparison across plots). (d) The parameters from part b plotted as a function of density, and (e) the slope of Q as a function of the speed at the given k. (f) Repeating part e for each station.

slowest vehicle will always be strictly free flowing. Of course, being the slowest vehicle also means that no matter what vehicle is ahead, that lead vehicle will travel faster and give rise to an expanding void in front of the subject vehicle. This expanding void is simply a long headway that is growing longer. At the other extreme, the vehicle with the fastest  $v_{FP}$  will eventually catch up to its leader and will begin car following as it joints (or forms) a moving queue behind that vehicle with a slower  $v_{FP}$ . For all other vehicles in between, they will exhibit a mix among these two extremes, either strictly free flowing at their  $v_{FP}$  or being stuck in a moving queue traveling slower than their  $v_{FP}$ , depending on the speed of their current leader. A long headway does not necessarily mean that a vehicle has a low  $v_{FP}$ , e.g., a long headway can arise behind a vehicle that leaves the lane, but if that happens, the follower will either quickly catch up to their leader (e.g., Wang and Coifman, 2008; Xuan and Coifman, 2012) or settle in to their own  $v_{FP}$  with a large headway.

For the sake of the present work, it does not really matter whether a vehicle with a long headway is closing or expanding the void ahead, what matters is that a vehicle with a long headway is likely to be traveling at their particular  $v_{FP}$ , and thus, is not likely to be very responsive to their leader. We will adopt the threshold of  $h \ge 3$  sec and v > 20 mph from Ponnu and Coifman (2017) to identify the free flowing long headway vehicles, *LHV*. This range of headways extends well beyond the distance where a human could perceive changes in spacing to a lead vehicle (e.g., Braunstein and Laughery, 1964; Duckstein et al. 1970; Mortimer, 1971) and it is safe to assume that a good portion of the LHV were able to travel at their preferred free speed for the ambient conditions. For simplicity, any vehicle with a headway below the 3 sec threshold is called a short headway vehicle, *SHV*. Some SHV might be traveling at their respective  $v_{FP}$ , which is fine, the 3 sec threshold is not meant to catch all of the strictly freely flowing vehicles, rather, it is meant to isolate a portion of the traffic that is almost entirely composed of vehicles that are strictly freely flowing, independent of their respective leaders.

The range and distribution of  $v_{FP}$  appears to determine both the shape of the qkFD and the prevalence of moving bottlenecks. In turn, the range of  $v_{FP}$  depends on the ambient conditions. Fig. 4b shows that during the non-HOV period most drivers choose a  $v_{FP}$  close to the speed limit, but during the HOV period there is a much larger range of  $v_{FP}$ . Ponnu and Coifman (2017) found that during the HOV period some free flowing drivers in lane 1 respond to ambient congestion in lane 2 by choosing their  $v_{FP}$  well below the speed limit, while other drivers under the same conditions continue to choose much higher  $v_{FP}$ . As a result, the HOV period sees a much larger range of  $v_{FP}$  in lane 1 compared to the non-HOV period.

The lane 1 vehicles collectively exhibit a concave qkFD during the HOV period with relatively small scatter when taken by fixed sampling period (Fig. 5a) or a well-defined curve when taken individually, independent of arrival order (circles in Fig. 5c). By

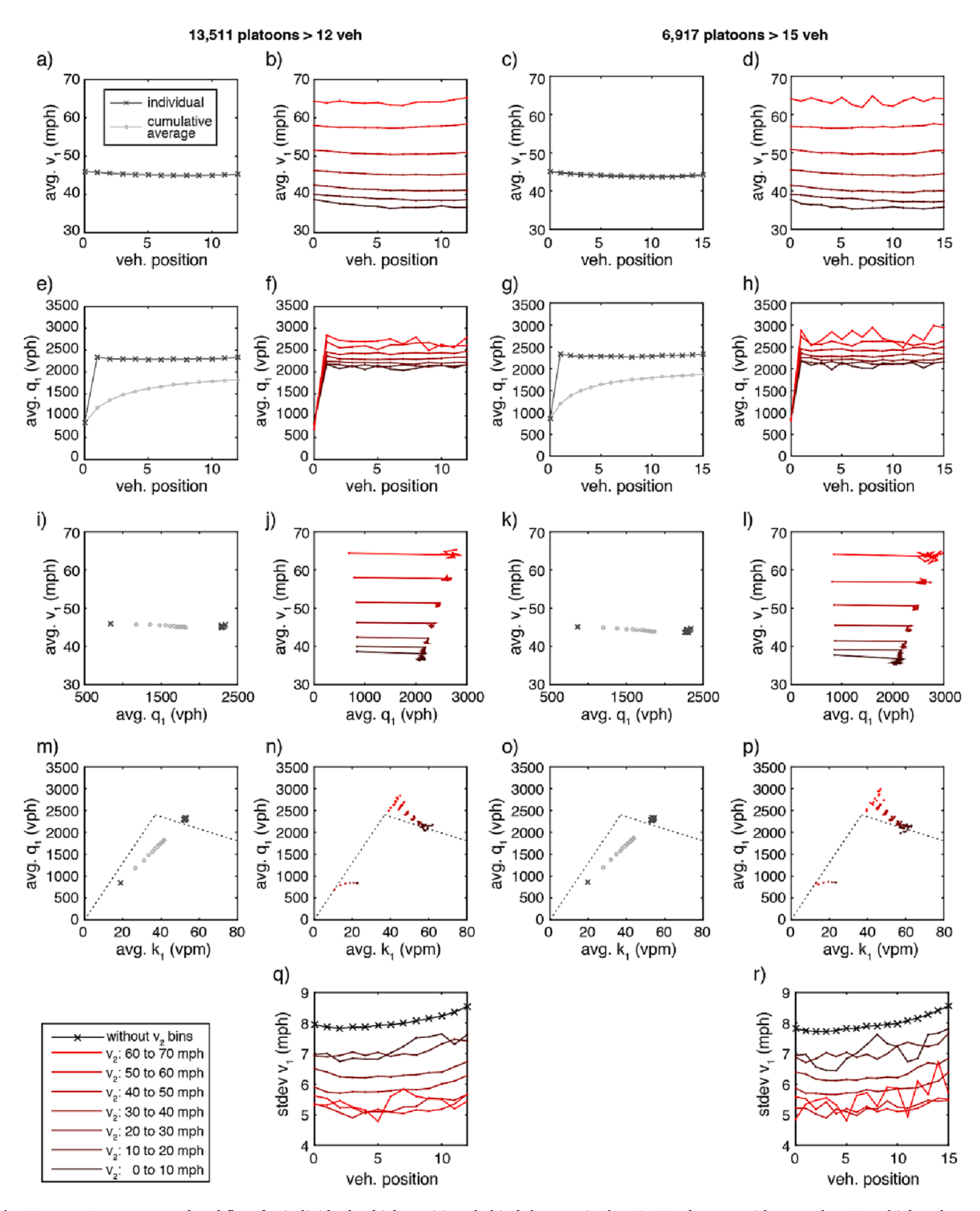


**Fig. 6.** Lane 1 average speed and flow for individual vehicle positions behind the LHV in the 13,511 platoons with more than 12 vehicles, the LHV as vehicle 0, and WITHOUT binning by  $v_2$ , (a) Average  $v_1$  by SHV vehicle position behind the LHV and cumulative average across all positions up to the given position, (e) the corresponding average  $q_1$ , note how the cumulative average slowly approaches that of the nearly constant individual values, but even by position 12 the cumulative average is still 22 % below the individual SHV (i)  $v_1$  versus  $q_1$ , (m)  $q_1$  versus  $k_1$  (dashed line for reference to compare across plots). (b) (f) (j) and (n) repeat the comparison only now binning by  $v_2$ . The right two columns of plots repeat the comparisons again, but this time using just the 6,917 platoons with more than 15 vehicles. Standard deviation of  $v_1$  by position in the queue behind the LHV at position 0 for platoons with more than (q) 12 vehicles, and (r) 15 vehicles.

conventional measures, one would likely consider Fig. 5a to be as close to "stationary" as one might hope to be able to achieve with real traffic data. But the collective behavior can be misleading, it does not mean that the individual vehicles are homogeneous. Fig. 5c shows two additional curves, the exact same analysis used to derive the circles from all vehicles was applied strictly to the LHV in the data set, yielding the bottom curve on the plot, and again to strictly the SHV in the data set, yielding the top curve on the plot. The curves for the LHV and SHV are very far apart, with the curve from all of the vehicles combined falling in between. The LHV account for about 28% of the observations in the combined curve. The LHV curve shows a positive correlation between q and k that is consistent with the free flow regime. The SHV, on the other hand, exhibit a negative correlation between q and k, and display a pattern that appears to come from the congested regime of a triangular qkFD.

The conflicting slopes of the qkFD for the LHV and SHV in Fig. 5c suggest that some of the vehicles are freely flowing and some are queued. If all vehicles keep their  $\nu_{FP}$ , then as the prevailing speed drops most vehicles will transition from the LHV curve at high prevailing speeds to the SHV curve at lower prevailing speeds, e.g., a vehicle with  $\nu_{FP}=65mph$  would fall on the LHV curve for  $\nu>65$  mph and the SHV curve for  $\nu<65$  mph. Thus, at the highest v the combined curve in Fig. 5c is close to the LHV curve and as v drops, the combined curve moves closer to the SHV curve.

This general idea of different vehicle classes combining to give rise to a concave qkFD has been theorized in the literature (e.g., Kesting et al., 2007). In fact, different vehicle classes like this are often viewed as being a pressure that increases the frequency of lane change maneuvers. If the adjacent lanes were all operating in the free flow regime, one would expect the different vehicle classes to naturally sort themselves by lane, and thus, pull the emergent qkFD in a given lane back to a triangular shape by simply reducing the distribution of  $v_{FP}$  in each lane (e.g., Daganzo, 2002). At some point though, demand can rise high enough that the fastest vehicles cannot escape being trapped behind slower vehicles. As a result, the free flow regime of the qkFD pulls away from triangular at high flows (e.g., Li and Zhang, 2011). In the present study, the faster vehicles in lane 1 cannot escape slower leaders by changing lanes because lane 2 is traveling much slower. So the moving bottlenecks behind slow moving freely flowing vehicles become a binding constraint at much lower flows, and with that constraint, the qkFD pulls away from a triangular shape because the voids ahead of the moving bottlenecks pull the aggregate flow below what could be sustained by homogenous vehicles at the given speed.

While the general idea of multiple vehicle classes combining to give rise to a specific shape of the qkFD is not new, the idea that the different classes interact in such a way to nullify the assumed stationarity necessary for LWR and SwA is a key insight of the present work. As noted in Section 1.2, in the free flow regime of a concave qkFD both LWR and SwA predict that signals must travel upstream in vehicle sequence, but the void ahead of an LHV will terminate any such signals.

The void ahead of the LHV also has a major impact on the net traffic state in samples containing LHV and SHV. Fig. 5c has simply sorted the vehicles by LHV and SHV, which obscures how the two classes impact the average state. To explore the combined impact on the sample, using the same set of vehicles from Fig. 5c, we now sort the SHV by arrival order after the most recent LHV. The first SHV behind each of these 18–22 ft LHV is selected as a group, then the second SHV behind each of the LHV, and so on until the next LHV is encountered. The LHV is denoted as n=0, first follower as n=1, second follower as n=2, and so forth. A LHV and all of its followers are retained if they come from a platoon meeting or exceeding a threshold number of vehicles, NT. The average  $v_1$  and  $q_1$  are found for each position up to n=NT and then  $k_1$  is calculated from the fundamental equation. This research considered four values of NT: 5, 8, 12 and 15 veh, to capture a range of moving queue lengths. In total, there were 83.5 k platoons for NT = 5, 36.2 k for NT = 8, 13.5 k for NT = 12 and 6.9 k for NT = 15. These totals are inclusive, so all of the platoons counted at NT = 15 are also counted for the smaller values of NT. In this manner, less than 8.3 % of platoons longer than 5 veh are also longer than 15 veh.

The results for the two largest values of NT are shown in Fig. 6 (the smaller NT's yielded similar results and thus, are omitted for brevity). The left-most column of plots shows the case for platoons with at least 12 SHV behind the LHV and ignores any SHV from the 13th onward. Fig. 6a shows the mean  $v_{svp}$  for each position. The curve is almost flat across all positions. For each position we calculate the cumulative average q, k and v across that position and all previous positions, so the cumulative average for the n-th position is taken across individual positions 0 to n. For speed, the two curves fall roughly on top of each other in Fig. 6a. Fig. 6e shows the mean  $q_{svp}$  behind the LHV with black x's for the individual position and a gray o's in position n for the cumulative average flow inclusive of all positions between 0 and n. The individual position  $q_{svp}$  more than doubles from n=0 to n=1, drops slightly to n=2 and then remains roughly constant as n increases further. The cumulative average flow starts out at less than half that of the SHV then slowly increases with diminishing returns for each successive position and converges toward the individual SHV flows as n increases. This gray curve shows the impact of the single LHV at the head of the moving queue, if the cumulative average excluded the LHV in position 0, it would fall close to the mean  $q_{svp}$  for all of the SHV positions (1–12). Even by the 12th position behind the LHV the cumulative flow with the LHV is 22 % lower than that of any of the SHV taken individually.

Fig. 6i shows the results in the speed-flow plane, once more using black x's for individual and gray o's for cumulative averages. The slightly higher speed of the LHV is evident with the left-most point, the individual SHV cluster together on the far right, and the curve of cumulative averages spans the range in between, moving to the right as n increases. Finally, Fig. 6m projects these results into the qkFD plane, and here too, as one moves further back in the moving queue, the closer the average state gets to the stable SHV state. So the LHV starts out at a flow much below the LHV, then as more SHV are included the curve moves towards the purely SHV state, but as already noted, even after 12 SHV the cumulative average q with the LHV is 22 % that of the SHV. This point is important because only

<sup>&</sup>lt;sup>6</sup> Technically the speed drops by about 1 mph from the LHV at n=0 to the follower at n=10, and then shows a small increase for the last two vehicle positions. Given the possibility of sampling biases we would be reluctant to impart any meaning on this small drop, but it could merit a deeper exploration using vehicle trajectory data. For this study the feature we ultimately want to show is that the general trends are consistent over a large range of  $\nu_2$ , so we did not investigate this small speed drop any further.

16.1% of the platoons longer than 5 veh were also longer than 12 veh, i.e., most moving queues should never even get this close to the flow that could be sustained by purely SHV at the given speed. Hence, the circles of the combined curve in Fig. 5c falling well below the corresponding SHV curve in that plot. The third column of plots in Fig. 6 repeats the analysis only now using platoons of at least 15 SHV behind the LHV and ignores any SHV from the 16th onward (these  $15 + \log$  platoons are all included in the platoons of at least 12 followers). The results are similar to those for the platoons with at least 12 SHV. In Fig. 6g the cumulative flow climbs slightly by the 15th SHV, now falling just 20 % below that of the pure SHV.

On average, the SHV in the moving queues appear to be able to sustain high  $q_1$  and  $v_1$  even though the traffic state for positions n greater than 0 is in the congested regime. The upshot is that the central tendency is surprisingly stable throughout the platoons of SHV, with tailgaters largely preserving the LHV speed. There does not appear to be much difference between successive positions over the first 15 SHV in the moving queues. These plots show that the neither the SHV nor LHV exhibit trends that are particularly close to those of the 5 min samples even though the 5 min samples appear to yield a reproducible pattern. The vehicles underlying the concave shape in Fig. 5a come from mixed conditions, with a few freely flowing LHV with low  $v_{FP}$  followed by many queued SHV. While the congested SHV are more numerous than the LHV, the emergent qkFD from the 5 min samples is concave and falls within the free flow regime.

In other words, we have just seen the building blocks that appear to violate stationary traffic conditions in a concave qkFD. The 5 min samples retain many of the traits of the LHV, where a small number of LHV dominate the dynamics of the entire traffic stream. As shown by the cumulative averages with the gray circles in Fig. 6e, 6i and 6 m, the large voids ahead of the LHV also pull the aggregate traffic state away from the flows that can be sustained by the SHV at a given speed, e.g., a moving queue of 13 vehicles remains 22 % below the q that purely SHV can achieve at the same speed.

#### 2.1.2. Influence of the adjacent lane

The inherent non-stationarity of the aggregate states is an important finding, but there is another dynamic at work that is equally surprising. Section 1.3 briefly reviewed recent research that has shown the qkFD can change shape in response to the adjacent lanes. As we will see in Section 2.2.3 the qkFD can make this shape change very rapidly, going from one extreme to the other in Fig. 2b in only a few seconds. These rapid qkFD fluctuations are far below the resolution of conventional vehicle detectors, which sample the traffic

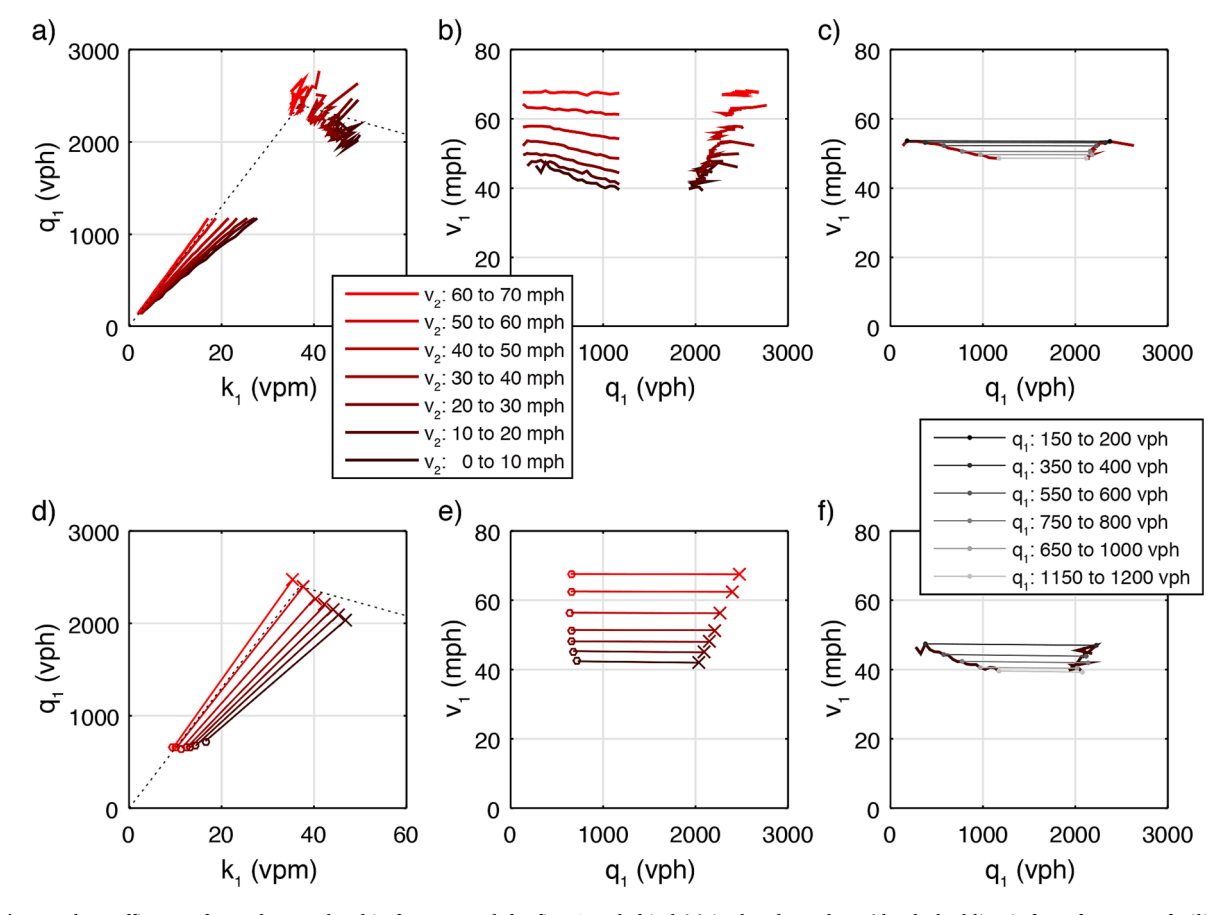


**Fig. 7.** The traffic state for each  $q_1$  and  $v_2$  bin for LHV and the first SHV behind (a) in the qkFD plane (the dashed line is for reference to facilitate comparison across plots), and (b) in the vqFD plane. (c) Repeating the  $v_2$ : 30–40 mph bins from part b, only now connecting the LHV and SHV with a straight line for every fourth  $q_1$  bin to illustrate the fact that speeds remain nearly constant for the leaders and followers. (d) Finding the median of all points in a given  $v_2$  bin from part a: "o" for LHV and "x" for SHV, (e) Repeating part d in the vqFD plane. (f) Repeating part c for  $v_2$ : 0–10 mph.

over 10's to 100's of seconds. We will get to the travel velocity of the transition in later sections, in this section we simply want to illustrate the underlying mechanics.

Before we get to the new findings with the SHV, we need to briefly review what is already known about the LHV from from Ponnu and Coifman (2017). Specifically, we strictly consider the LHV passenger vehicles from all 70 days at all six stations during the HOV period using the svp measurements from Equations 3–6. The vehicles are binned by  $L_{svp}$ , only retaining  $18ft < L_{svp} < 22ft$ . Any vehicle with  $v_{syp}$  < 20 mph was discarded as those vehicles could have come from the congested regime. The remaining vehicles were then binned by  $q_{SVD}$  for 50 vph bins, only retaining those vehicles falling between 0 and 1,200 vph; and finally they were binned by the speed of the adjacent lane preceding vehicle,  $v_2$ , in 10 mph increments. At this point, any individual bin with fewer than 100 vehicles is discarded to ensure the sample sizes are sufficiently large enough to be representative. For the remaining bins the harmonic mean speed,  $v_1$ , and median flow,  $q_1$ , were found and then  $k_1 = q_1/v_1$  was calculated for the given  $q_1$  and  $v_2$  bin. After this processing just over 289,000 vehicle actuations in lane 1 on I-80 met the LHV binning criteria for the HOV period. The left side of Fig. 7b shows the resulting curves for the LHV in the speed-flow plane, vqFD (for the moment ignore the curves for  $q_1 > 1200vph$ ). The curves go successively from fastest to slowest  $v_2$  bin as one moves from top to bottom in this plot. The fan of vqFD curves is readily apparent, with the speed-intercept and slope both decreasing as  $v_2$  decreases. All but the fastest  $v_2$  bin show that  $v_1$  drops as a function of  $q_1$ , which is characteristic of a concave qkFD in the free flow regime; but the fact that this slope and the intercept of the vqFD drop as a function of the adjacent lane speed is absent from conventional traffic flow models. These FD are projected to the qkFD plane in the lower portion of Fig. 7a, and now as one moves from left to right the curves go successively from fastest to slowest  $v_2$  bin in this plot. The scope of Ponnu and Coifman (2017) was limited to the LHV, but LHV only represent 28 % of the vehicle arrivals.

With the brief review of the prior LHV work complete, we now move to the new research on the SHV. Each SHV immediately behind an LHV is paired to the LHV and they are both binned by the LHV svp measurements. In the event that two LHV pass successively then the first LHV is excluded from Fig. 7. While the SHV svp measurements are not used for binning, they are used to find median  $q_1$ , harmonic mean  $v_1$ , and calculated  $k_1$  for the vehicles in a given SHV bin. The net results for the first SHV behind a LHV are shown with the curves at  $q_1 > 1200vph$  in Fig. 7a-b. The SHV use the same shading as the LHV for a given  $v_2$  bin and follow the same pattern, e.g., the SHV curves go successively from fastest to slowest  $v_2$  bin as one moves from left to right in Fig. 7a. The SHV curves do differ from the LHV curves in one important manner, by definition the LHV  $q_1$  is that of the flow bin, whereas the SHV  $q_1$  could be anything since these vehicles were binned strictly based on the LHV ahead.

First, consider the general trends relating a given SHV bin to the corresponding LHV bin. To help see the patterns in the data, Fig. 7d shows the median of each qkFD curve in Fig. 7a, with the LHV median (o's) connected by a line segment to its corresponding SHV median (x's) for the given  $v_2$  bin. Note that the line segments do not overlap, the highest  $v_2$  bin is on the left and each successive  $v_2$  bin falls immediately to the right of the curve from the  $v_2$  bin above. Projecting these curves into the vqFD plane, Fig. 7e, one can see that the median SHV speed matches that of the median LHV speed for the given  $v_2$  bin. In other words, the first SHV behind the LHV has matched its leader's speed even though the headway is much smaller. As a result, the SHV  $q_1$  is higher, with several of the individual SHV bins exceeding 2,500 vph in Fig. 7a. Returning to Fig. 7d, the median  $q_1$  for the LHV's stays roughly constant across the  $v_2$  bins even though  $v_1$  drops with  $v_2$ . On the other hand, the x's corresponding to the SHV bins trace out a progression with slope equal to -39 mph as  $q_1$  drops with  $v_2$ , and this negative correlation between flow and density is consistent with these points coming from the congested regime of a triangular qkFD.

To see greater detail of the relationship between SHV and preceding LHV, Fig. 7c pulls out a single pair of LVH + SHV curves from Fig. 7b to compare the vqFD curves for a single  $v_2$  bin (30–40 mph in this case). On the left one can see that  $v_1$  drops as  $q_1$  increases for the LHV. Each point on the LHV curve has a corresponding point on the SHV curve, as shown with a connecting line for every fourth bin pair. The line segments are consistently close to zero slope; thus, within a given  $v_2$  group the LHV speed drops as  $q_1$  increases, and the SHV matches this speed. Also note that the SHV show decreasing  $q_1$  as  $v_1$  drops. This process was repeated in all  $v_2$  bins with similar results, as illustrated in Fig. 7f for the slowest  $v_2$  bin (0–10 mph).

Summarizing the trends in Fig. 7: generally, the SHV match their leading LHV  $v_1$  regardless of  $v_1$ ,  $q_1$ , or  $v_2$ , so their speed is determined by their leader. Meanwhile, they take lower  $q_1$  in response to decreasing  $v_1$  or  $v_2$ . In other words, the first SHV behind an LHV appears to behave as if they are in a moving queue and the SHV are sensitive to the adjacent lane speed.

The relationships shown in Fig. 7 are not limited to the first SHV behind a LHV. Expanding the analysis to consider the LHV as n = 0, first follower to be n = 1, second follower n = 2, and so forth, the second column of subplots in Fig. 6 show the case for platoons with at least 12 SHV behind the LHV and ignores any SHV from the 13th onward. In other words, the second column of plots is simply an expansion of the first column of plots (analyzed in the previous section) to also take into account the adjacent lane speed. To simplify the already complicated plots in this case the LHV are all grouped together, i.e., they are not sorted by  $q_1$  bins, and the cumulative average results used in the previous section are omitted to keep the plots readable. Vehicles are binned by both the position behind the LHV and the corresponding  $v_2$  seen by the given vehicle, yielding the family of curves. Fig. 6b shows the mean  $v_{svp}$  for each position in each  $v_2$  bin, with the top curve corresponding to the fastest  $v_2$  bin and then each successive curve corresponding to the next  $v_2$  bin. The  $v_1$  curves for  $v_2 \ge 30mph$  are roughly flat across n in Fig. 6b but show a slight decreasing trend of a few mph in  $v_1$  between n = 0 and n = 12. This trend is larger for the lowest three  $v_2$  bins, but still the total drop does not exceed 3 mph. So, in general as n increases, the SHV roughly maintain the  $v_1$  of the LHV. Fig. 6f shows the mean  $q_{svp}$  for each position behind the LHV. Once more, the top curve corresponding to the fastest  $v_2$  bin and each successive curve corresponding to the next  $v_2$  bin with the exception of occasional noise that pulls the curves out of order for a given n. The individual position  $q_{svp}$  increases by a factor of 3 or 4 from n = 0 to n = 1, reflecting the LHV to SHV transition. This plot shows that  $q_1$  drops with  $v_2$ , but remains high and roughly constant across n for the SHV in a given  $v_2$  bin. Fig. 6j projects the points from the previous two plots into the v

qkFD plane. These two plots show that the relationships found for the first SHV behind the LHV in Fig. 7 also hold for the subsequent SHV followers, i.e., the SHV match the speed of the leader and maintain a high flow, but  $q_1$  still drops with  $v_1$  and  $v_2$ . On average the platoons appear to be able to sustain high  $q_1$  and  $v_1$  even though the traffic state for positions n>0 is in the congested regime. The upshot is that the central tendency is amazingly stable throughout the platoons of SHV, with tailgaters largely preserving the LHV speed. But as one moves further back in the platoons to higher n, Fig. 6q shows the corresponding standard deviation of  $v_1$  increasing as n increases. In other words,  $v_1$  becomes less stable, potentially indicating the initial formation of upstream moving disturbances in  $v_1$  within a given platoon that can lead to slow-and-go or stop-and-go waves if the platoon were long enough.

The fourth column of plots in Fig. 6 repeats the analysis only now using platoons of at least 15 SHV behind the LHV and ignores any SHV from the 16th onward. The results are similar to those for the platoons with at least 12 SHV, with the exception that some curves show greater noise due to the smaller sample size. Summarizing the trends in Fig. 6, for the platoon following the LHV, there does not appear to be much difference between successive positions over the first 15 following SHV. Similar to Fig. 7, Fig. 6j and 6l show that for the most part followers in each position are able to match the speed of its given leader, independent of  $v_1$ ,  $q_1$ , or  $v_2$ , but throughout all positions n behind the LHV, the SHV take lower  $q_1$  in response to decreasing  $v_1$  or  $v_2$ , and thus, the SHV exhibit a positive correlation between  $q_1$  and  $v_1$ , consistent with the congested regime. Collectively, Figs. 7 and 6 show that both LHV and SHV are sensitive to the speed in the adjacent lane, both groups of vehicles take a lower speed in response to lower speeds in lane 2. On average, the LHV do not change their flow (headway) much in response to speeds in lane 2, while the SHV exhibit lower flow in response to lower speeds in the adjacent lane, consistent with moving to a lower speed in the congested regime of the qkFD.

#### 2.2. Measuring the propagation velocity of traffic state signals

Up to this point the analysis has only considered the shape of the qkFD seen at detector stations. This section begins by considering the velocity at which signals should travel in accordance to LWR and SwA, then the various subsections proceed to measure how fast signals actually travel between detector stations.

According to the fundamental equation, v=k/q, vehicles should travel at a speed equal to the slope of the radial connecting the traffic state on the qkFD curve to the origin, as illustrated by the sample traffic state with subscript x in Fig. 5b for lane 1 at station 2. Meanwhile, as noted in Section 1.1, according to LWR signals and disturbances arising from small variation of the traffic state should travel with a slope equal to the tangent of the qkFD curve at the given traffic state,  $c=\frac{dQ_1(k_1)}{dk_1}$ , also illustrated for the sample point x in Fig. 5b. Fig. 5d shows the resulting  $v_1$  and  $\frac{dQ_1(k_1)}{dk_1}$  as a function of  $k_1$ , e.g., when  $k_1$  is 20 veh/mi,  $v_1$  is about 58 mph and  $\frac{dQ_1(k_1)}{dk_1}$  is about 40 mph, and throughout the range of  $k_1$ ,  $\frac{dQ_1}{dk_1} \le v_1$ . Fig. 5e shows  $\frac{dQ_1(k_1)}{dk_1}$  as a function of  $v_1$ , with a slope of 2 in this case due the second order fit. This progression to Fig. 5e was repeated independently for each of the six stations, with the net results shown in Fig. 5f. The concave qkFD shape was seen at every station, but the parameters vary between stations. Fig. 5f shows that  $c=\frac{dQ_1}{dk_1}>0$  and  $v_1\gg c$  in the operating range of this study, thus, if LWR holds, signals will travel downstream in space slower than the vehicles via Equation (2). Meanwhile, if SwA holds, when the state fluctuates between two points on the free flow regime of a concave qkFD, Equation (1) will yield a signal velocity u that is much slower than the slowest  $v_1$  of the two states.

In short, if LWR or SwA hold for the free flow regime of the qkFD (e.g., Fig. 5a-b), signals should travel downstream in space slower than the traffic. Section 1.2 argued that the dynamics that give rise to the concave qkFD likely violate the necessary assumption of stationarity for these classical traffic flow models to hold, Section 2.1.1 has shown evidence of such disruptions. To investigate the outcome of this conflict, Section 2.2.1 measures the dominant velocity at which signals in  $q_1$  (demand) propagate downstream, henceforth denoted with  $w_{q1}$ . Section 2.2.2 extends the analysis to measure the dominant velocity at which signals in  $v_1$  propagate downstream, denoted with  $w_{v1}$ . Meanwhile, Section 2.1.2 showed evidence of the FD changing shape in response to the adjacent lane and Section 2.2.3 extends the analysis to explore evidence of induced signals from the adjacent lane.

#### 2.2.1. The velocity of signals in demand

This section takes the time series flow from pairs of successive detector stations to investigate what direction and how fast signals propagate between the two stations. Fig. 3 shows the six detector stations used to collect the data set, yielding five pairs of successive stations, as listed in the first pair of columns in Table 1, where station 7 is furthest upstream and the station numbers decrease as one moves downstream. To find the speed of propagating signals between a given pair of stations the work follows Coifman and Wang (2005) in that the time series data at one station is shifted against the corresponding time series at the other station to find the time offset yielding the highest correlation coefficient. The resulting dominant signal velocity is simply the quotient of the distance between the two stations (as listed in Table 1) and the optimal time offset.

More formally, the analysis uses 30 sec samples for greater fidelity compared to the 5 min samples used in the earlier sections. The time series flow is found at the downstream station for the time window of 16–18 h on a given day (recall that the HOV period spans 15–19 hrs). Then a slightly larger time window is found at the upstream station such that there are 5 min before and after the downstream time window, i.e., 15:55 to 18:05. The extra 5 min on either end ensures that the time series of the upstream station can be shifted up to 5 min to the left or right with reference to the downstream station's time series while providing a full two hours to measure the correlation coefficient. This 5 min window was chosen because the optimal time offset rarely exceeds 1 min. The downstream station has a single time series, but the upstream data are aggregated separately 30 different times, with a start of 0, 1, 2, ..., 29 sec offset relative to the downstream start time. Thus, the upstream aggregation will start on the second at 15:55:00, 15:55:01, ..., 15:55:29. Each of these 30 time series starting at different times are stored as a separate column in a matrix. To retrieve data

**Table 1**The signal velocity at maximum correlation for the plots in Fig. 8 for 16:00 to 18:00 hr on Sept. 16, 1999.

sta	tions	distance (ft)	Lane 1							
			signal velocity $w_{q1}$ from flow correlation (mph)	$\begin{array}{c} \text{downstream} \\ \text{station} \\ \text{med}(v_1) \text{ (mph)} \end{array}$	VRI Link speed $med(v_{Link}) \\ (mph)$	downstream station total flow (vph)	VRI Link inflow % of total flow			
7	6	1100	57.7	48.4	48.4	1309	2.3 %			
6	4	3500	61.2	50.0	50.9	1401	6.8 %			
4	3	1800	45.5	51.1	41.0	1351	-4.6 %			
3	2	1500	46.5	48.9	48.4	1349	-0.1 %			
2	1	1500	48.7	52.0	47.8	1360	1.4 %			

starting after the first 30 sec, one need only ignore the number of rows at the start of the matrix corresponding to the integer number of 30 sec sample periods after 15:55:00. This process allows for one second time step in shifting while preserving the 30 sec aggregation period. To find the correlation between two time series we need the same number of data points in each series. The downstream aggregated data have 240 points over the two hour window. So, successive 240 time points are selected from the upstream time series starting at each sec between 15:55:00 and 16:05:00, leading to a total of 600 different upstream time series each with 240 data points. Then the correlation coefficient of the static downstream station's time series with each of the 600 upstream time series is found via Equation (7), where U & D are respectively the time series of the upstream and downstream stations, Cov(U, D) is the covariance of U & D, and  $\sigma_U$  &  $\sigma_D$  are respectively the standard deviations of U & D. These 600 data sets at the upstream station are in fact akin to taking a 30-sec moving average with 1-sec increments and they represent a time lag at the upstream station over the range: -300 to 300 sec.

$$\rho_{UD} = \frac{Cov(U, D)}{\sigma_U \sigma_D} \tag{7}$$

This analysis was conducted on five different days, consider the following results from a typical day. Fig. 8a shows the correlation coefficient of the flow time series at each time shift for traffic in lane 1 traveling from station 2 to station 1, with the peak at a shift of 20 sec. This process in lane 1 is repeated in each pair of stations on this day, shown in the remaining subplots in Fig. 8 and the resulting dominant signal velocities,  $w_{q1}$ , are recorded in Table 1. For reference the table also shows the median speed at the downstream station for the two hour period. But the local speeds do not capture conditions between the detector stations. So borrowing the idea of vehicle reidentification, VRI, (Coifman, 2003a; Coifman and Cassidy, 2002) this work manually reidentified distinct long vehicles (L > 28ft) as they pass successive stations to capture conditions between stations. On this day each link had at least 34 vehicles in lane 1 reidentified between the detector stations over the 16-18 hr time period, with a maximum of 52 vehicles reidentified in a given link. The median link speeds from the reidentified vehicles are shown in Table 1, with only one link showing a signal velocity below the median VRI link speed, and that exception is still within 2 mph. The results were similar across all five days that were studied, as summarized in Table 3. Across all five days and all five links, 22/25 of the outcomes show  $w_{a1}$  either exceeds or is within 2 mph of the median VRI link speed. Meanwhile, the o's in Fig. 9 show that for all links on this day  $w_{q1}$  is above the calculated  $\frac{dQ_1(k_1)}{dk_1}$  for the bounding stations at the prevailing median link speed for the given stations. The x's in this figure repeat the comparison, only now using the median downstream station speed. Across all five days and all five links, 23/25 of the outcomes show  $w_{q1}$  is faster than the corresponding  $\frac{d\Omega_1(k_1)}{dk_1}$ . These results show that  $w_{a1}$  appears to travel with the traffic, supporting the hypothesis that the LHV are able to travel at their preferred speed and as a result of the void in front of the LHV, signals in flow (demand) travel downstream with the vehicles rather than according to LWR or SwA.

Up to this point the evaluation has not considered the number of lane change maneuvers. After reidentifying vehicles to measure the VRI link speed, using the technique of Coifman (2003b) the matched vehicles also allow the measurement of the inflow to lane 1, where inflow is defined by Equation (8). The inflow does not capture all lane change maneuvers, just the total change in number of vehicles between the upstream and downstream stations between a successive pair of reidentified vehicles. Tables 1-3 show the net inflow as a percentage of the downstream flow. Although not shown, the net inflow to lane 1 on a given link and day appears to maintain a roughly constant rate over the 2 hr period. Table 3 shows that the net inflow on a given link is roughly consistent across days. After taking the median by link, link 6 to 4 shows the maximum inflow at +6.2%, while link 4 to 3 shows the minimum inflow at

<sup>&</sup>lt;sup>7</sup> This processing was limited to the five days presented herein, all of the other days in the data set exhibited a time offset error of about 15 sec at station 4. This error can be identified by plotting the individual vehicle lengths versus time and shifting one time series L by the free flow travel time during the off-peak periods. The offset could be fixed on any given day by simply adding the corresponding time shift to the station 4 data, but that would create uncertainty as to whether the shift unknowingly impacted the findings. As a result, we do not employ such a correction. It appears that the station 4 time offset error sets in at the start of each day. If station 4 restarts during the day (as evident by a period of no data lasting several minutes) for the five days used in this section the time offset error goes away for the remainder of the day, only to return at the start of the next day. The 70-day data set come from the very beginning of the BHL deployment. This offset error at station 4 appears to have been resolved shortly after the time period of the data set. However, for consistency with the earlier work we chose to use the same data set. Regardless, one should be cautious of this issue if expanding the analysis to other days in the data set.

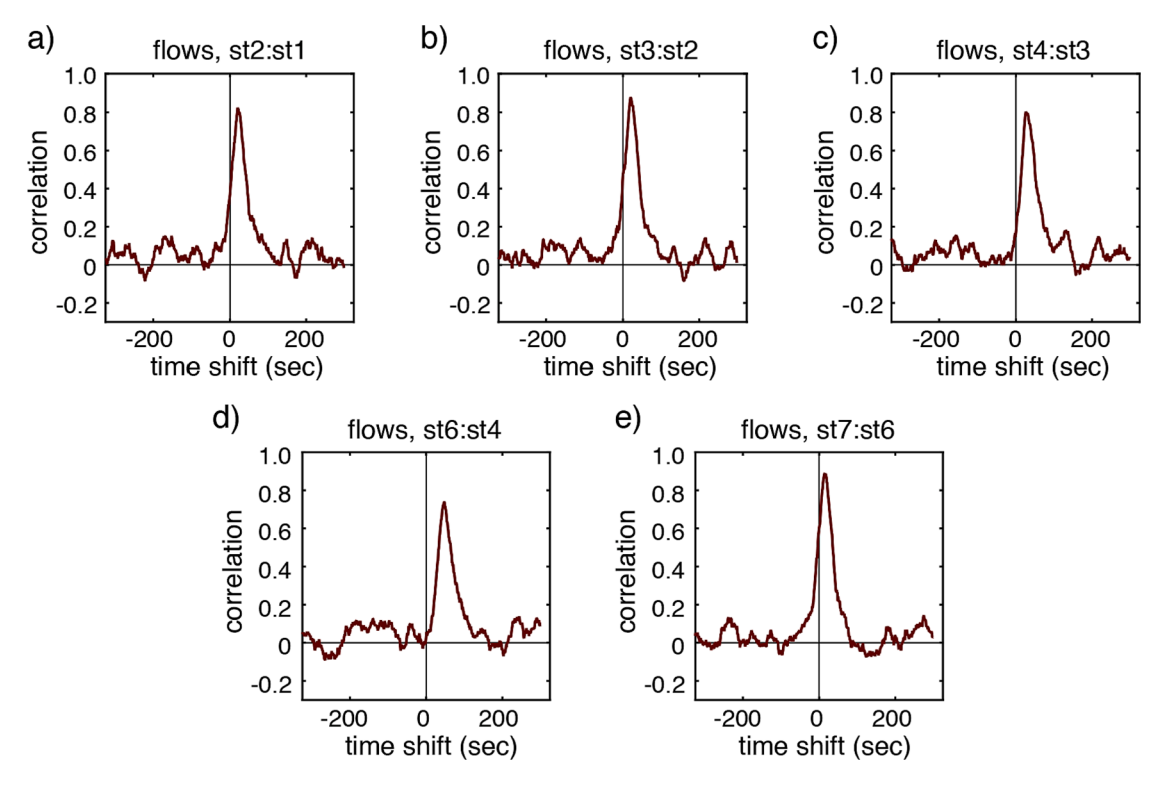


**Fig. 8.** Time series correlation of  $q_1$  in lane 1 between successive stations on a typical day (Sept. 16, 1999), for stations: (a) 1 & 2, (b) 2 & 3, (c) 3 & 4, (d) 4 & 6, (e) 6 & 7.

**Table 2**The signal velocity at maximum correlation for the plots in Fig. 11 for 16:00 to 18:00 hr on Sept. 16, 1999.

stati	ons	distance (ft)	Lane 1							Lane 2	
			signal velocity (mph)		downstream station	VRI Link speed	downstream station	VRI Link inflow	signal velocity (mph)		
			speeds $w_{v1}$	flows $w_{q1}$	med(v <sub>1</sub> ) (mph)	$med(v_{Link})$ (mph)	total flow (vph)	% of total flow	speeds $w_{v2}$	flows $w_{q2}$	
7	6	1100	50.0	57.7	48.4	48.4	1309	2.3 %	-12.1	-13.2	
6	4	3500	47.7	61.2	50.0	50.9	1401	6.8 %	-12.4	-13.0	
4	3	1800	27.3	45.5	51.1	41.0	1351	-4.6 %	-12.7	-14.3	
3	2	1500	37.9	46.5	48.9	48.4	1349	-0.1 %	-10.3	-11.2	
2	1	1500	30.1	48.7	52.0	47.8	1360	1.4 %	-11.6	-11.1	

**-4.2 %.** 

$$inflow = total entrances - total exits$$
 (8)

The open circles in Fig. 10 show the resulting  $w_{q1}$  as a function of inflow for all five stations on all five days. While the points are grouped by station in this illustration, a linear fit was applied to all 25 of the points collectively, resulting in the fit line shown in the figure. The slope of the fit line shows that the correlated signals are also influenced by the inflow to the lane. The more vehicles that enter the lane between stations, the faster the signals travel (consistent with earlier studies, e.g., Zhang, 2003). While more advanced traffic flow models can accommodate the inflow, it is beyond the assumptions of the classical LWR and SwA, and so the performance of these theories are further degraded. However, the inflow is not the dominant factor because even on links with near zero (st3 to st2, and st2 to st1) or negative inflow (st4 to st3) still exhibit  $w_{q1}$  faster than the signal velocity predicted by LWR and SwA. Meanwhile, although the nature of the data precludes studying overtaking directly, one should recognize that lane change maneuvers and inflow are the realization of overtaking.

#### 2.2.2. The velocity of signals in speed

The results in Section 2.2.1 indicate that demand appears to travel downstream with the LHV, but that is not the whole story of what is going on in the traffic stream. In this section we repeat the correlation analysis in lane 1 except using time series speed at the

**Table 3**The signal velocity at maximum correlation for five days. Across all days each link had at least 27 long vehicles reidentified over the given 2 hr period, with a maximum of 52 long vehicles reidentified in a given link on a given day.

stations		date (yymmdd)	Lane 1							Lane 2	
			signal velocity (mph)		downstream station	VRI Link speed	downstream station	VRI Link inflow	signal velocity (mph		
			speeds $w_{v1}$	flows $w_{q1}$	median(v <sub>1</sub> ) (mph)	med(v <sub>Link</sub> ) (mph)	total flow (vph)	% of total flow	speeds $w_{v2}$	flows $w_{q2}$	
7	6	990,913	34.1	62.5	50.2	51.8	1271	3.3 %	-11.2	-13.2	
		990,916	39.5	50.0	48.4	48.4	1309	2.3 %	-12.1	-13.2	
		990,917	53.6	39.5	45.9	46.0	1382	3.7 %	-12.3	-12.1	
		990,923	46.9	57.7	48.6	52.6	1255	3.0 %	-12.3	-12.5	
		991,014	50.0	57.7	49.2	52.3	1201	1.3 %	-12.5	-12.3	
6	4	990,913	35.1	58.2	53.9	53.9	1325	4.5 %	-13.0	-12.6	
		990,916	37.3	50.8	50.0	50.9	1401	6.8 %	-12.4	-13.0	
		990,917	36.7	55.5	47.9	52.7	1464	6.2 %	-12.5	-12.7	
		990,923	45.0	51.9	49.6	52.2	1328	5.8 %	-12.6	-12.6	
		991,014	47.7	61.2	51.1	59.9	1291	7.1 %	-11.6	-12.2	
4	3	990,913	29.2	49.1	54.6	46.0	1272	-4.2 %	-12.9	-12.7	
		990,916	43.8	47.2	51.1	41.0	1351	<b>-4.6 %</b>	-12.7	-14.3	
		990,917	30.7	42.3	48.1	39.7	1412	-3.8 %	-12.5	-13.5	
		990,923	36.1	43.8	50.9	42.7	1281	-3.5 %	-12.5	-13.6	
		991,014	27.3	45.5	51.1	47.7	1237	-4.2 %	-13.1	-13.8	
3	2	990,913	37.9	51.1	51.4	50.8	1283	1.1 %	-10.8	-11.6	
		990,916	31.0	51.1	48.9	48.4	1349	-0.1 %	-10.3	-11.2	
		990,917	28.4	46.5	45.0	45.6	1417	0.7 %	-11.2	-12.8	
		990,923	37.9	51.1	47.9	46.4	1285	0.5 %	-10.2	-9.6	
		991,014	37.9	46.5	48.7	48.3	1236	0.1 %	-13.6	-13.0	
2	1	990,913	35.3	44.5	54.6	48.9	1301	1.3 %	-11.9	-13.1	
		990,916	42.6	51.1	52.0	47.8	1360	1.4 %	-11.6	-11.1	
		990,917	29.2	44.5	49.2	43.6	1418	0.1 %	-11.4	-11.2	
		990,923	29.2	46.5	51.9	47.3	1301	1.7 %	-12.8	-11.9	
		991,014	30.1	48.7	51.8	47.8	1254	1.4 %	-10.8	-13.6	
7	6	median	46.9	57.7	48.6	50.4	1271	3.0 %	-12.3	-12.5	
6	4	median	37.3	55.5	50.0	52.7	1328	6.2 %	-12.4	-12.6	
4	3	median	30.7	45.5	51.1	42.7	1281	-4.2 %	-12.7	-13.6	
3	2	median	37.9	51.1	48.7	48.3	1285	0.5 %	-11.2	-12.6	
2	1	median	30.1	46.5	51.9	47.8	1301	1.4 %	-11.4	-11.9	

pair of stations instead of flow. The resulting correlations are shown with dark curves in Fig. 11, where the speed results for a given link are shown in a plot above the flow results for the same link, e.g., Fig. 11a shows the speed correlation results for the link between stations 1 & 2 directly above Fig. 11d where the dark curve reiterates the flow correlation results from Fig. 8a. For the moment ignore the lighter curves. The peak correlation of the dark curves are used to establish the dominant velocity for signals in speed for lane 1,  $w_{\nu 1}$ . The resulting  $w_{\nu 1}$  are shown in Table 2 for the sample day and Table 3 for all days. Throughout the days and links  $w_{\nu 1}$  are consistently lower than  $w_{q1}$ .

The slower signal velocity for  $w_{v1}$  is not a surprise. This process of using correlation to find the dominant signal velocity should yield a higher dominant signal velocity from time series q than it does from time series v for the given pair of stations because the correlation equation is most sensitive to the extreme values in the time series, and these extremes happen in one region of a concave FD for q and a different region of the concave FD for v. To understand why, consider the hypothetical concave FD in Fig. 1 (bold curves), where Fig. 1b shows the qkFD and Fig. 1a shows the same FD in the speed-flow plane (transposed from conventional practice so that q is on the vertical axis, to facilitate comparisons with the qkFD). The intervals AB and CD in Fig. 1a show that if the traffic state fluctuates between A and B it exhibits  $|\Delta v| = 3mph$  and  $|\Delta q| = 300vph$ . Whereas, if the traffic state fluctuates between C and D it exhibits  $|\Delta v| = 9mph$  and  $|\Delta q| \approx 100vph$ . The time series correlation is sensitive to the magnitude of the fluctuations in the signal, either  $\Delta v$  or  $\Delta q$ . Since v and q are intrinsically linked via the FD, the correlation of time series q will give greater weight to lower flow conditions like interval AB; while the correlation of time series v will give greater weight to higher flow conditions like interval CD. If the signals travel with the traffic the q correlation should yield  $w_{q1}$  that is faster, corresponding to the higher speeds of low flow conditions, e.g.,  $v_A$  or  $v_B$  in Fig. 1, while the v correlation should yield  $w_{v1}$  that is slower, corresponding to the lower speeds of the traffic under higher flow conditions, e.g.,  $v_C$  or  $v_D$ .

Tables 2 and 3 show that  $w_{v1}$  is slower than  $w_{q1}$ , and thus, closer to the signal velocities that would be predicted by LWR and SwA, but the  $w_{v1}$  results still generally support of our argument. As per Fig. 9, the diamonds show  $w_{v1}$  at the median VRI link speed and for 10/10 of the point & curve pairs (two in each plot)  $w_{v1}$  fall above the bounding station  $\frac{dQ}{dk}$ . Meanwhile, the "+" shows the same  $w_{v1}$  at the median downstream station speed, and only 7/10 of the corresponding point & curve pairs have  $w_{v1}$  falling above the bounding station  $\frac{dQ}{dk}$ . Because of the aforementioned correlation biases, one should expect the signals to travel with the vehicles and the vehicles to exhibit a range of link speeds, with the true average link speed falling between  $w_{v1}$  and  $w_{q1}$ . Briefly considering the impact of lane

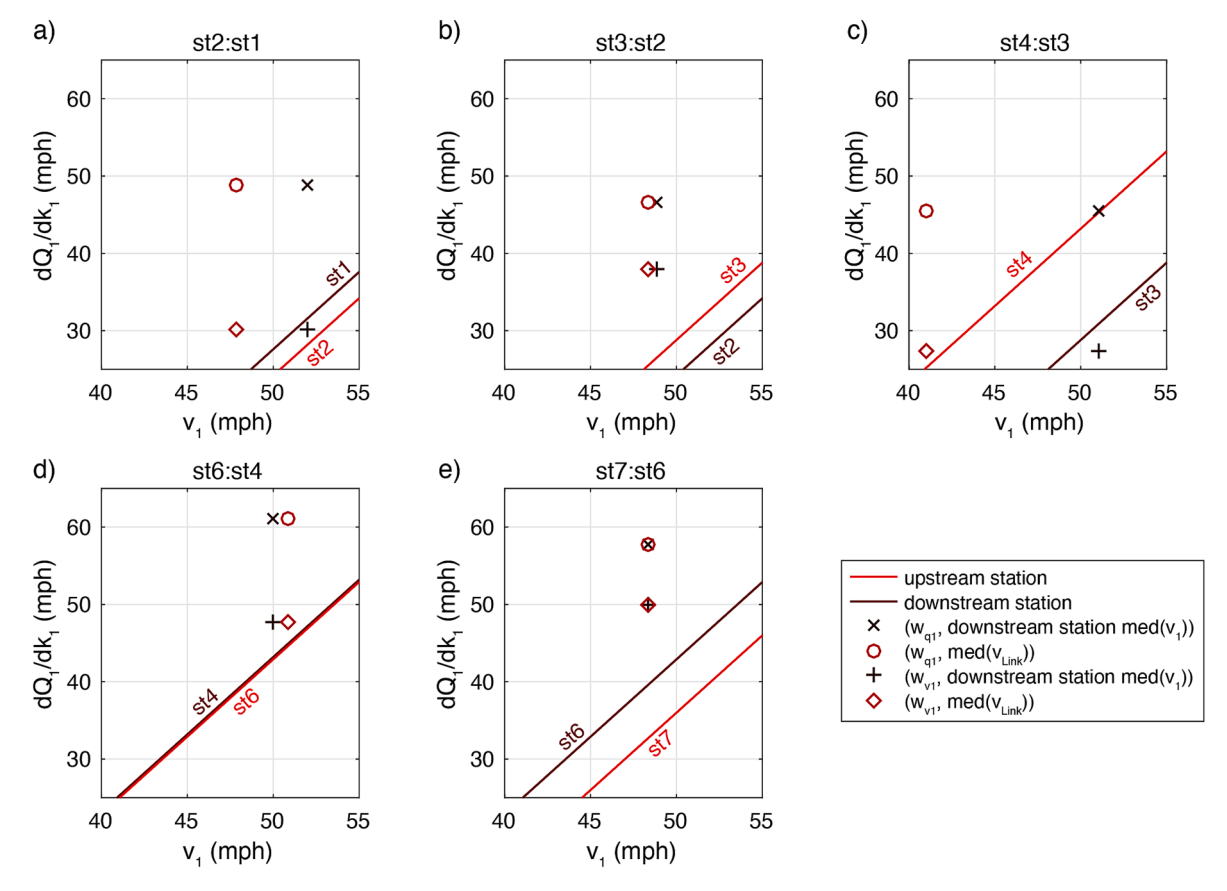


Fig. 9. Measured signal velocities  $w_{q1}$  and  $w_{v1}$  plotted at the median speed at the downstream station and median link speed from reidentified vehicles for each link on Sept. 16, 1999. Each plot also repeats dQ/dk as a function of  $v_1$  for the bounding detector stations from Fig. 5f.

change maneuvers via the net inflow, the bottom set of points (large solid circles) in Fig. 10 show the resulting  $w_{v1}$  as a function of inflow for all five stations on all five days. Like  $w_{q1}$ , a linear fit was applied to all 25 of the points collectively, resulting in the fit line shown in the figure. Aside from the y intercept being 13 mph slower, the results from  $w_{v1}$  are very similar to  $w_{q1}$  from Section 2.2.1.

While the mechanism of the slower  $w_{v1}$  is not as strong as  $w_{q1}$ , the signals in  $q_1$  and  $v_1$  traveling with the vehicles is an important finding, showing that the LHV violate the assumptions of LWR and SwA; as a result, even though the qkFD is concave the dominant signals in demand appear to travel with the vehicles at this site. As noted previously, this finding does not rule out the possibility of shorter lived signals that propagate upstream through the moving queues, most of which will never last long enough to be seen at two successive stations given the typical moving queue lengths seen here (e.g., less than 8.3 % of platoons longer than 5 veh are also longer than 15 veh).

## 2.2.3. Influence of the adjacent lane

The lane 1 speed correlation curves in Fig. 11 show another curious feature, subplots a, b, and g show a well-defined second mode indicative of an upstream moving signal, while the single mode for lane 1 in subplot c is more diffuse than the other links suggesting a second mode that overlapped the primary mode. The prospect of signals propagating upstream in the free flow regime is completely unexpected. It is also notable that these signals are only evident in speed, the corresponding correlations of flow show no indication of secondary modes with negative travel times. In an effort to understand these upstream moving signals in lane 1, the lighter curves in Fig. 11 repeat the correlation in flow and speed for lane 2, the adjacent GP lane that is congested during the study period. In both speed and flow the peaks in the Lane 2 curves indicate upstream moving signals, as should be expected for congested traffic. There is no indication of secondary modes in lane 2. The resulting signal velocities for lane 2, denoted  $w_{v2}$  and  $w_{q2}$ , are shown in Table 2 and Table 3. The signal velocities in lane 2 are consistent with the signal velocities from Coifman and Wang (2005). Fig. 11 shows that the secondary modes from the lane 1 speed correlation roughly align with the corresponding singular modes from lane  $w_{v2}$  and  $w_{q2}$ .

If traffic is strictly free flowing in lane 1, the signals should propagate strictly downstream when the qkFD is static since Equations (1) and (2) will strictly yield positive velocities in the free flow regime (downstream moving signals). On the other hand, if the traffic state in lane 1 was propagating upstream due to congestion, then it should be reflected in all dimensions of the traffic state, i.e., it should include evidence of upstream moving signals in the  $q_1$  correlation but they are only seen in the  $\nu_1$  correlations. Examining all 6 detector stations, we found the correlation between the unshifted  $\nu_1$  and  $\nu_2$  at the given station, and in all cases the interlane

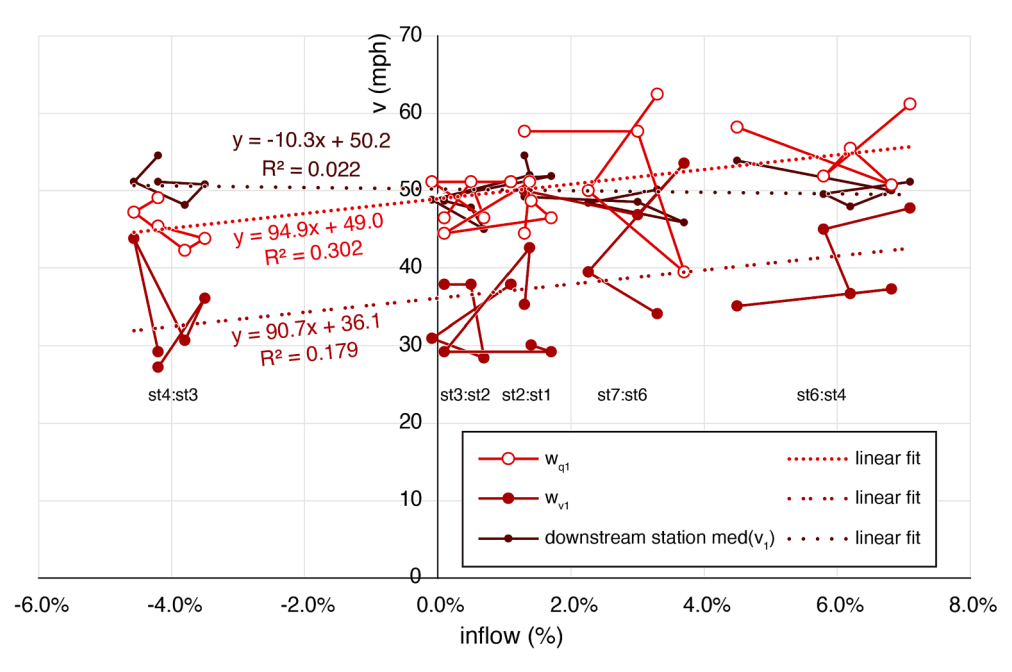


Fig. 10. Signal velocities  $w_{q1}$  and  $w_{v1}$  versus percent inflow from all five links and all five days (connected points show all data from a given link). For reference, the corresponding median speed at the downstream station is also shown. Linear regression fit lines show that over the range of observed inflow the signal velocities systematically vary over a range of about 10 mph, while the downstream station speeds are almost constant, with a range of about 1 mph.

correlation coefficient was on the order of 0.45 for the time series speeds in the two lanes. This local interlane speed correlation coefficient value for the downstream station is shown with a horizontal dashed line in the speed correlation plots of Fig. 11 and for all four of the links with evidence of a secondary peak in  $v_1$  correlation the local interlane correlation coefficient is comparable to the peak  $v_1$  correlation between successive stations. On the other hand, the flows appear to largely be independent of the adjacent lane with an interlane correlation coefficient on the order of just -0.02 between  $q_1$  and  $q_2$  at each station. So it appears that  $v_1$  is sensitive to  $v_2$ , but  $q_1$  is not sensitive to  $q_2$ .

The solution to this enigma follows from the insights presented in Section 1.3 and the interlane comparisons of Section 2.1.2. Since lane 2 is congested, signals in  $v_2$  propagate upstream at  $w_{v2}$ , the local changes in  $v_2$  at a given point in space induce a local disturbance in lane 1 that takes the motion illustrated in Fig. 2b, pulling lane 1 to a different qkFD curve without much impact on  $q_1$ . In other words, changes of  $v_2$  modulate which qkFD curve that lane 1 operates on, with little impact on  $q_1$  but a large impact on  $v_1$ . Since the waves in lane 2 pass different locations at different times, the induced signals in lane 1 move with the waves in lane 2. All the while, lane 1 remains in the free flow regime even though it exhibits the upstream moving disturbances induced from  $v_2$ .

To demonstrate these induced signals, consider the empirical data in Fig. 12. At first glance this figure is very busy, but each of the first four rows of subplots just present the same eight curves in different ways. This figure shows the time series speed and flow data from lanes 1 and 2 at two successive detector stations, specifically, station 4 upstream and station 3 downstream. The speed data are the individual vehicle speeds while the flow data are a 30 sec moving average at 1 sec time steps. Fig. 12a shows the speed in both lanes at station 3. For the most part speeds are around 55 mph in lane 1 and 40 mph in lane 2, but at 16.04 hrs both lanes see the speed drop by about 30 mph and then recover. Fig. 12b repeats the plot only this time for station 4, with the speed drop happening a little later, at about 16.06 hrs. This upstream moving disturbance is plainly evident when plotting the two speed time series from a given lane on the same axes, as shown in Fig. 12e-f for lanes 1 and 2, respectively. Fig. 12c-d show the concurrent flows at each station using the same line styles for a given lane and station. Unlike the speed data, at both stations there is no apparent linkage between the flow in the two lanes when the speed drop passes. Fig. 12h shows the two flow time series for lane 2, and like  $v_2$  in Fig. 12f,  $q_2$  is indicative of an upstream moving disturbance. This trend is absent from the corresponding plot for  $q_1$  in Fig. 12g, instead, the major transitions are indicative of downstream moving conditions.

To make these temporal relationships clearer, consider a moving time frame that travels with the disturbance in lane 2. We take just the 9 min of data shown at station 3 and find the time-shift for station 4 that maximizes the correlation between the two  $v_2$  time series in lane 2 (Fig. 12f) and shift the station 4 data earlier by this amount in Fig. 12i-l, i.e., the third row of plots in Fig. 12 simply repeats the second row of subplots after shifting the station 4 data earlier to align the speed drop in lane 2. Visually, the large displacements in the lane 1 speeds align well between the two stations after making the time shift (Fig. 12i) and similarly for the lane 2 flows (Fig. 12l). This time shift corresponds to u = -12.3mph, consistent with typically reported signal speeds in congestion (see, e.g., Coifman and Wang, 2005). Repeating this process only now using the lane 1 flows in Fig. 12g and the 9 min of data shown at station 3, we find the time shift for station 4 that maximizes the correlation between the two  $q_1$  time series in lane 1, the results are shown in Fig. 12m-p, with Fig. 12o

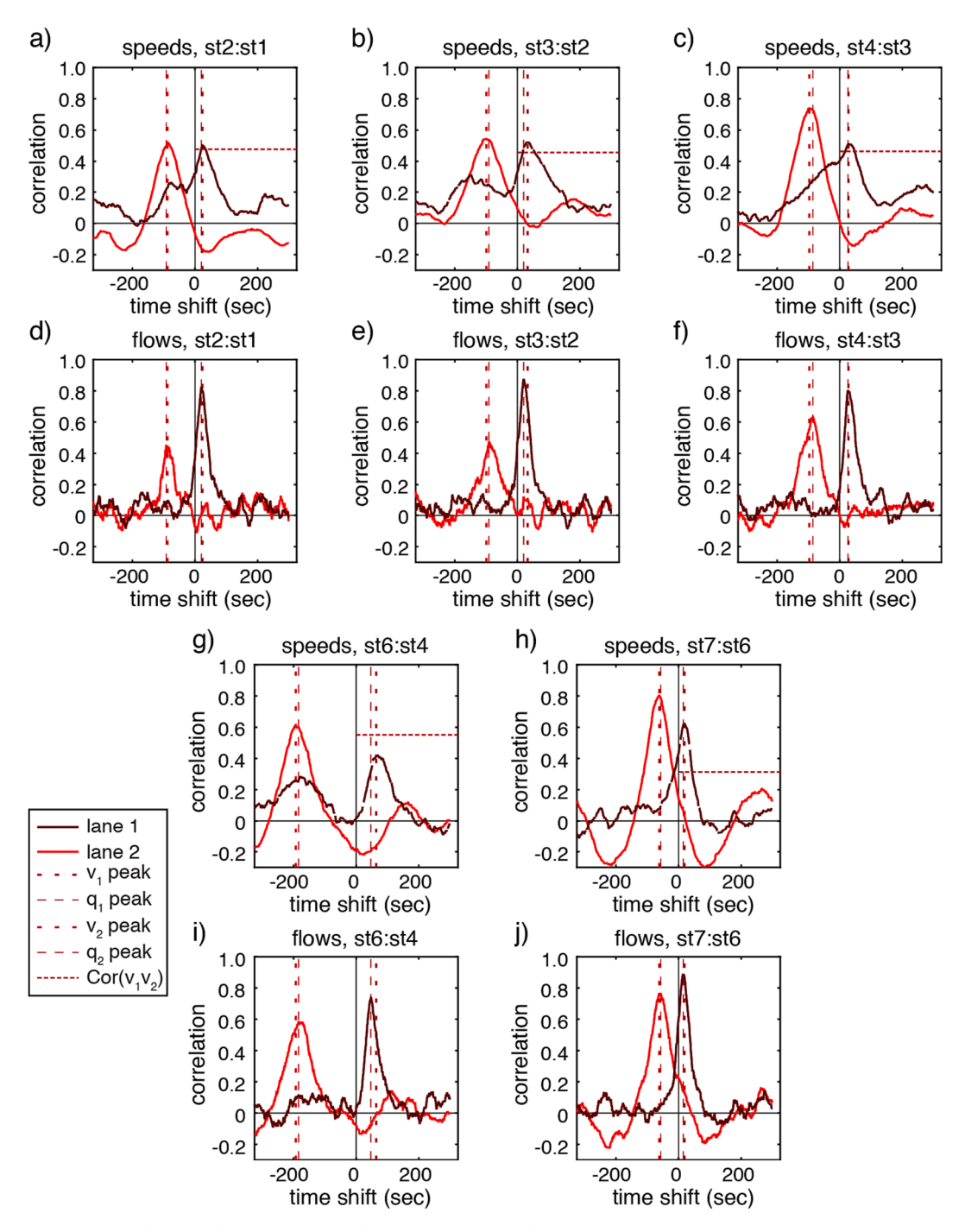
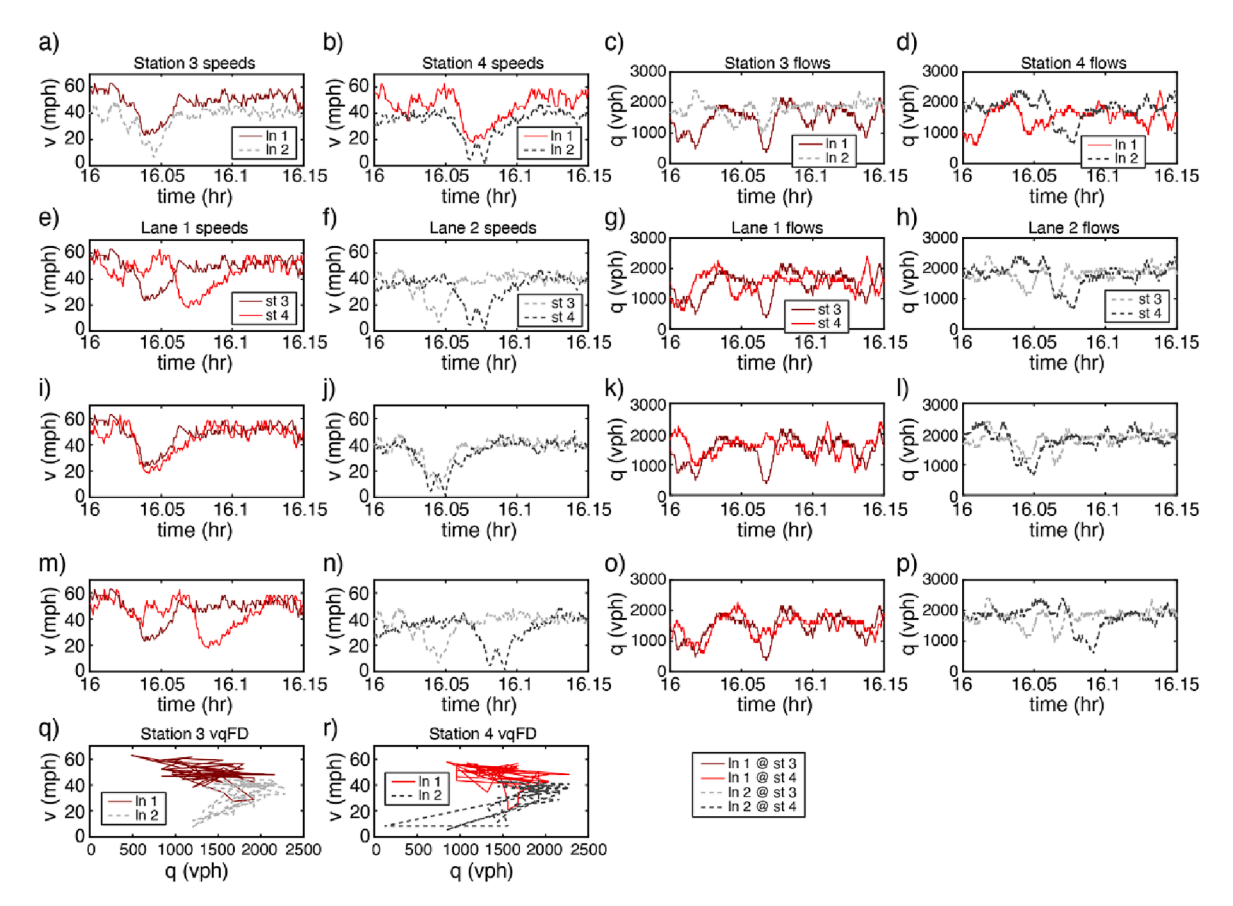


Fig. 11. Time series correlation in lane 1 and separately in lane 2 of speeds between successive stations on a typical day (Sept. 16, 1999), for stations: (a) 1 & 2, (b) 2 & 3, (c) 3 & 4. Of flows between stations: (d) 1 & 2, (e) 2 & 3, (f) 3 & 4. Of speeds between stations: (g) 4 & 6, (h) 6 & 7. Of flows between stations: (i) 4 & 6, (j) 6 & 7. The time shift of each peak for a given pair of stations is indicated with dashed lines on the given matching pair of speed and flow plots. The speed plots include a horizontal line showing the  $\nu_1, \nu_2$  correlation coefficient at the given downstream station.

clearly showing evidence to support downstream moving traffic conditions. For reference, Fig. 12q-r show the corresponding v versus q from 30 sec samples from 10 min before to 10 min after the time range shown in Fig. 12a-d. At both stations the lane 1 data show high speeds and a negative sloped trend consistent with free flow conditions in a concave vqFD, while the lane 2 data show lower speeds and a positive sloped trend consistent with congested conditions. So here we have an upstream moving signal in lane 1 speed, concurrent with a disturbance in lane 2, even though lane 1 is otherwise consistent with operating in the free flow regime.



**Fig. 12.** Detailed case study of signals propagating between stations 4 (upstream) and 3 (downstream) on Sept. 17, 1999. Lane 1 mostly exhibits uncongested speeds, but drops briefly when a large speed drop passes in lane 2 at (a) station 3, and a short time later at (b) station 4. The corresponding flows at (c) station 3 and (d) station 4. Replotting the speeds this time by station in (e) lane 1, (d) lane 2. The corresponding flows in (g) lane 1, and (h) lane 2. (i-1) repeating plots e-h only shifting all curves from station 4 upstream by  $w_{v2}$  calculated from plot f. (m-p) repeating plots e-h only now shifting all curves from station 4 by  $w_{q1}$  calculated from plot g. Throughout lane 1 is shown with solid lines and lane 2 with dashed lines. (q-r) the corresponding 30 sec average vqFD for the two lanes at each station (including 10 min on either side of the time range shown in a-d).

The induced disturbances do not always propagate between stations though. Fig. 13 repeats the analysis between stations 2 and 3 on a different day. This time, Fig. 13b shows that the lane 1 drivers at station 3 do not appear to respond to the speed drop in lane 2. As a result, when shifting the lane 1 speeds at station 3 earlier in Fig. 13i there is no apparent propagation of the disturbance in lane 1 speeds. Fig. 14 shows that this same disturbance in lane 1 station 2 can re-establish itself by the time the corresponding lane 2 disturbance reaches station 4. In this case, the figure repeats the analysis from Fig. 13 for the exact same time period except the upstream station is now set to station 4. Fig. 14b shows the speed in lane 1 at station 4 responds to the speed drop in lane 2. After finding an upstream time shift corresponding to u = -13.6mph from Fig. 14f as used in Fig. 14i-l, we see in Fig. 14i that lane 1 also exhibits an upstream moving disturbance in speed that travels at the same velocity. Yet this disturbance was not evident at the intervening station (Fig. 13i), so the disappearance and reemergence adds further evidence that the disturbance in lane 1 speed was induced from the lane 2 disturbance. Ergo, for these signals in  $v_1$  to propagate upstream like this in the free flow regime, the qkFD must rapidly change shape in response to  $v_2$ , as per Fig. 2b, or combining the impacts of  $q_1$  and  $v_2$  as shown in Fig. 2c.

One might argue that a wide moving jam, WMJ, could create a similar upstream moving drop and recovery in  $v_1$  (see, e.g., Laval, 2007). But if the lane 1 disturbance were due to a WMJ, the entire traffic state in lane 1 should reflect the changing traffic state and  $q_1$  does not appear to change. There are several other factors that indicate the signals are not due to a WMJ. WMJ's can only propagate if the initial state is near capacity flow, in which case the recovery wave will travel at about the same velocity as the initial drop (see, e.g., Coifman and Kim, 2011). Yet Figs. 12-14 consistently show that the lane 1 flows are far below those seen in lane 2. When the initial traffic state is far below capacity like this, SwA dictates that the speed drop will propagate upstream much slower than the recovery wave since the jam should discharge at capacity flow and so the queue will dissipate from downstream in a manner similar to traffic discharging from a queue at a stop light. Then of course the possibility of a WMJ is further contradicted by the fact that the lane 1 speed drop was seen at stations 2 and 4 (Fig. 14i), but not the intervening station 3 (Fig. 13i).

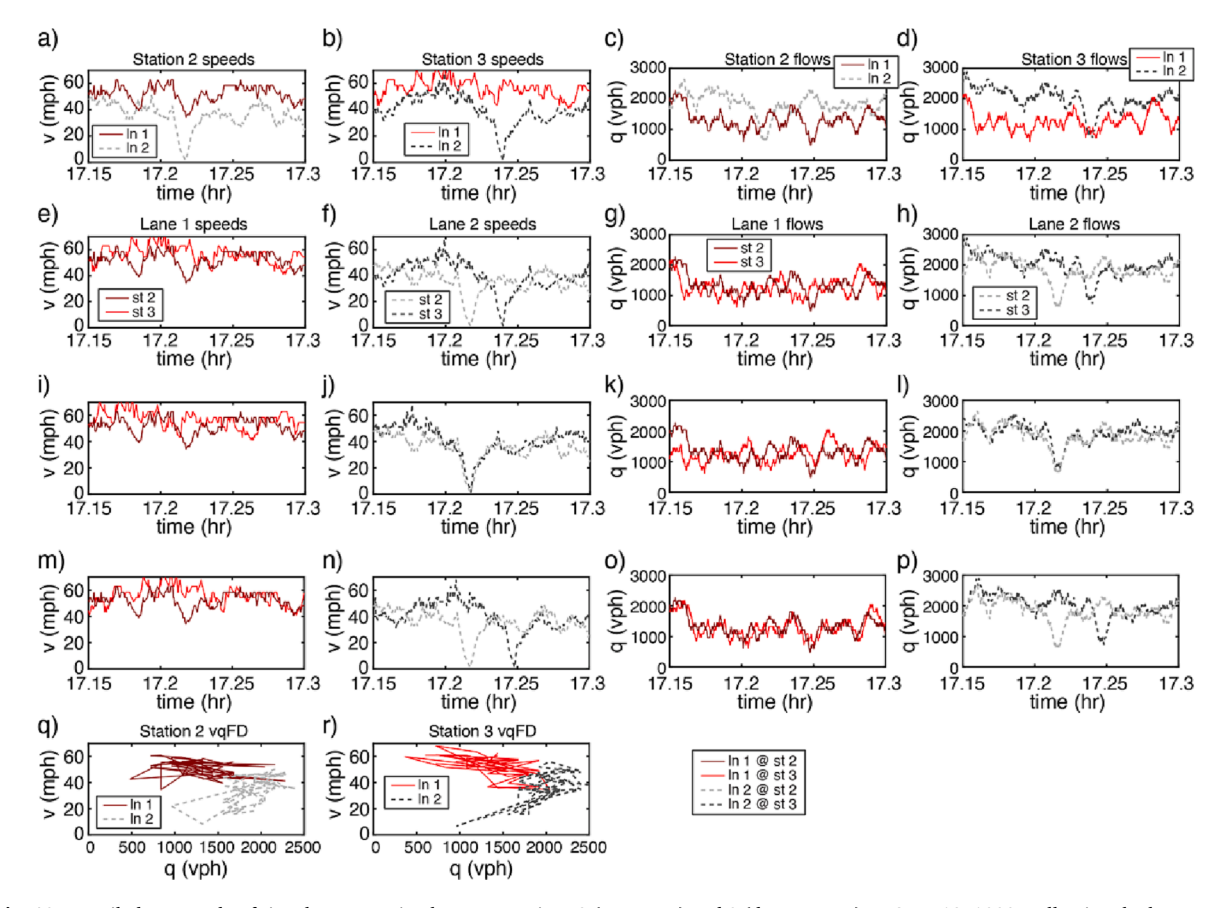


**Fig. 13.** Detailed case study of signals propagating between stations 3 (upstream) and 2 (downstream) on Sept. 13, 1999. Following the layout and format of Fig. 12. Unlike the earlier example, part i shows little evidence of an upstream moving signal in lane 1 speeds.

#### 3. Discussion and conclusions

Classical SwA and LWR theories applied to the free flow regime of a concave qkFD predict that fluctuations in traffic state should propagate downstream in space slower than the traffic speed at the given traffic states. These theories assume that traffic is stationary and thus, as signals travel downstream in space they travel upstream in vehicle sequence. This paper has shown that at the study site the traffic dynamics that give rise to a reproducible concave fundamental diagram, also systematically disrupt the stationarity of the traffic flow, which in turn, violates the assumptions necessary to apply LWR or SwA to the concave shaped qkFD.

Consider point x in Fig. 5b. Conventional wisdom says that this reproducible point on the qkFD represents a stationary state, or at least a sufficiently near stationary state that LWR and SwA should apply. Implicit in this assumption is that all the vehicles in the sample are close to the average speed, headway, and spacing, or at very least, they are all operating in the free flow regime. Yet when we dissect the data to look at the individual vehicles, we find that although the aggregate states fall on the concave qkFD, the underlying vehicles in a given sample are inhomogeneous, with a minority of freely flowing LHV that typically become moving bottlenecks and catch several SHV in moving queues. Taken individually, the LHV and SHV respectively yield the bottom and top curves in Fig. 5c. The LHV curve is consistent with the free flow regime, the SHV curve is consistent with the congested regime, and taking all of the vehicles together yields the middle curve that is not representative of either group taken individually. Yet this middle curve is very similar to the emergent qkFD from conventional 5 min samples in Fig. 5a-b.

To be clear, the general idea of moving bottlenecks is nothing new, but what is new is the idea that the concave shape in the qkFD emerges as a result of several such moving bottlenecks in a given sample. The moving bottlenecks are so small that several could pass in a typical 5 min sample of a vehicle detector and the voids last such a brief time that they are impossible to discern in the aggregated

<sup>&</sup>lt;sup>8</sup> Note that SwA predates LWR and applies in more conditions than LWR (see Section 1.2). Furthermore, throughout this paper when we discuss SwA, we mean SwA applied to macroscopic samples as reported by conventional vehicle detectors. These aggregate samples make no distinction for the start or end of discrete microscopic traffic states such as the void ahead of the LHV. If one has microscopic traffic data, then SwA can be used on a microscopic scale to correctly construct the evolution of the traffic state by allowing signals to capture the different vehicle speeds on either side of the void.

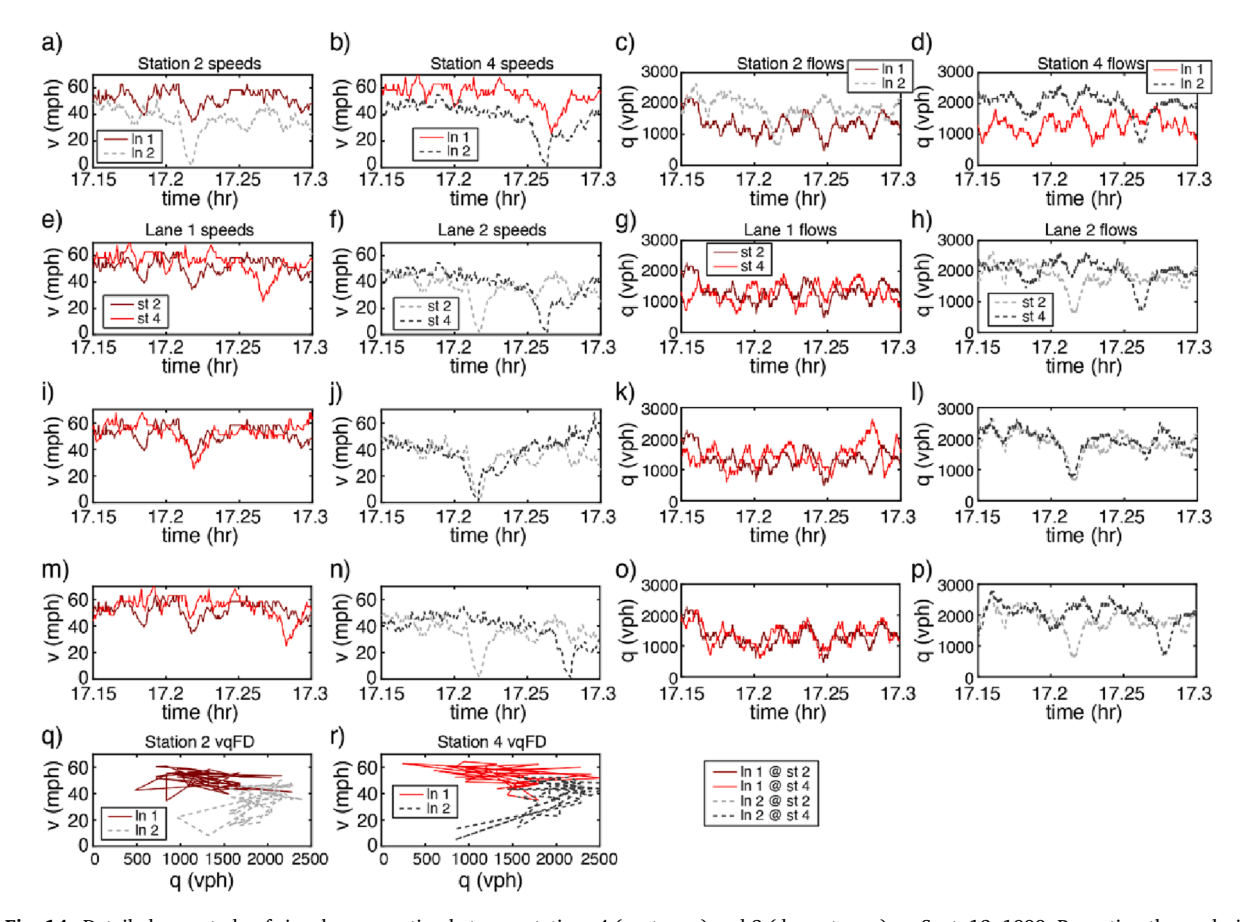


**Fig. 14.** Detailed case study of signals propagating between stations 4 (upstream) and 2 (downstream) on Sept. 13, 1999. Repeating the analysis from Fig. 13 for the same date and downstream station, but changing to a new upstream station (further upstream). Note the lane 1 disturbance in speed that was absent at station 3 in Fig. 13i has re-established itself at station 4 in part i of this figure.

data, e.g., a large void might last 10 s out of a 300 s sample. While the moving bottlenecks of the LHV are relatively frequent (LHV account for about 28 % of the vehicles), their moving queues tend to be much smaller than the number of vehicles seen in a typical 5 min sample (less than 8.3 % of platoons longer than 5 veh are also longer than 15 veh in Fig. 6). It is only in retrospect after microscopically dissecting the macroscopic data that we are able to see that the one macroscopic indicator of the voids is the fact that q (v) on the concave qkFD falls below that of a triangular qkFD (e.g., Fig. 1, Fig. 4c, Fig. 5c and Fig. 6m).

As shown in Section 2.1.1, it appears that the LHV dominate the dynamics of the entire traffic stream. On the one hand, the large void ahead of the LHV will terminate signals moving upstream in vehicle sequence that is necessary for LWR or SwA applied to a concave qkFD. On the other hand, as shown by the cumulative averages with the gray circles in Fig. 6e, 6i and 6m, the large voids ahead of the LHV also pull the aggregate traffic state away from the flows that can be sustained by the SHV at a given speed, e.g., on average the LHV and a moving queue of 12 SHV remains 22 % below the q that purely SHV can achieve at the same speed. The net impact in these data should be even larger since most platoons are shorter than 12 veh.

Sections 2.2.1 and 2.2.2 showed that indeed, the signals appear to travel much faster than predicted by LWA or SwA applied to the concave qkFD, e.g., Fig. 9 shows that for most links, the dominant signal from correlating time series flow is much faster than the signal velocity that would be predicted by LWR or SwA. Instead of obeying these classical traffic flow theories, the signals appear to be traveling with the vehicles, i.e., they are traveling with the LHV that are the moving bottlenecks. While this outcome is similar to the phenomena observed microscopically by Edie and Baverez (1967), as noted above, the new insight is that this appears to happen many times in a typical sample, so the occurrence is not apparent in typical aggregated traffic data even though it nullifies the assumptions of the macroscopic LWR and SwA models. As noted in Section 1.2, prior work has shown that the non-stationary dynamics arising from moving bottlenecks can be captured with more sophisticated models. But not all sophisticated models do so, e.g., many hydrodynamic models are like LWR and depend on signals strictly propagating upstream in vehicle sequence. The key point of the present work is that the classical LWR and SwA models do not appear to hold in the free flow regime of a concave qkFD because the traffic dynamics that give rise to the concave qkFD also violate the assumptions of these classic models.

<sup>&</sup>lt;sup>9</sup> A 30 sec sample is likely to be impacted similarly, but 30 sec samples are much noisier due to partial headways, etc.

Key finding #1: it appears that the very factors that give rise to a concave qkFD can also undermine the assumptions necessary to apply LWR or SwA to aggregate data in the free flow regime.

Key finding #2: by extension, any traffic flow model that depends on stationarity is potentially at risk of this same failure whenever a concave qkFD arises from dynamics that negate stationarity.

These findings should <u>not</u> apply to triangular qkFD, where signals in the free flow regime are already expected to travel with the vehicles. While the moving bottlenecks of the LHV appear to be the dominant factor in this corridor, they clearly are not the only mechanism that undermines LWR and SwA. Fig. 10 shows that the correlated signals are also influenced by the inflow to the lane. The more vehicles that enter the lane between stations, the faster the signals travel (consistent with earlier studies, e.g., Zhang, 2003). While more advanced traffic flow models can accommodate the inflow, it is beyond the assumptions of the classical LWR and SwA, and so the performance of these theories are further degraded. However, the inflow does not appear to be the dominant factor because even on links with near zero or negative inflow we still measure signal velocities comparable to vehicle speeds, and much faster than the signal velocity predicted by LWR and SwA (Fig. 9a-b and Table 3). Meanwhile, although the nature of the data precludes studying overtaking directly, one should recognize that lane change maneuvers and inflow are the realization of overtaking.

There is also clear evidence of a new factor that is counter to the assumptions LWR and SwA. Coifman and Ponnu (2020) demonstrated that the relative speed to adjacent lanes can systematically modulate the shape of the qkFD in the ego lane, and as a result, they postulated that changes to the shape of the qkFD will also be reflected in the emergent dynamics, i.e., the velocity at which signals propagate over space. However, that work only considered the shape of the qkFD and did not measure any actual signal propagation over space. The present work empirically demonstrates that indeed, induced distortions in the qkFD not only impact the signal velocity, they can give rise to induced signals in the ego lane that travel with disturbances in the adjacent lane. Although lane 1 appears to be operating in the free flow regime, and thus, the classical theories tell us that all signals should propagate downstream in space, Fig. 11 shows secondary peaks in the lane 1 speed correlations consistent with upstream moving signals in lane 2. These secondary peaks are not evident in the flow correlations. Fig. 7d shows the LHV roughly maintain the same flow but vary v in response to the adjacent lane. Fig. 12 shows an example of an induced signal propagating upstream through lane 1 traffic that is operating in the free flow regime. Figs. 13-14 shows an example of another upstream moving signal that dies out at one station but is then re-established at the next station upstream. While this paper has shown the induced signals in extreme conditions where the adjacent lanes are in different regimes, thereby making the induced disturbances readily observable, prior work has shown the underlying interlane dependencies transcend the HOV lane, persisting in GP lanes and when both lanes are operating in the same regime (Ponnu and Coifman, 2015; Ponnu and Coifman (2017); Coifman and Ponnu, 2020). The empirical revelation of the superposition of two or more signals is incompatible with hydrodynamic traffic flow models that assume a single characteristic signal reaches each point in time and space. In any event, for these induced signals to arise the qkFD must change shape very rapidly, going from one extreme to the other in Fig. 2b in only a few seconds. These rapid qkFD fluctuations are far below the resolution of conventional vehicle detector aggregation, which sample the traffic over 10's to 100's of seconds. Because the mechanism distorts FD itself, it should impact LWR, SwA or any other model that explicitly or implicitly incorporates some form of the FD. Future research is needed to determine how to handle a rapidly changing FD to account for these induced signals.

Key finding #3: Adjacent lanes impact signal propagation in the subject lane.

Key Finding #4: This study empirically found signals induced from adjacent lanes, giving rise to a superposition of signals in the subject lane.

Of course, this work only considered a single lane. If one expanded to multiple lanes and all drivers have the same preferred free speed, then the free flow regime should trace out the straight line of a triangular qkFD at that given free speed. This homogeneous  $v_{FP}$  situation typically happens by design, on many facilities the speed limit already forces the fastest lanes to a speed lower than the  $v_{FP}$  that many drivers would naturally choose on their own (see, e.g., Ponnu and Coifman, 2017). We speculate that a facility needs many drivers with their  $v_{FP}$  below the speed limit (or no speed limit) before a concave qkFD will arise, <sup>10</sup> and at least in the US, the general guidelines for setting speed limits typically prevents such a situation from arising.

Now consider the case where drivers do exhibit a range of  $v_{FP}$  on a multi-lane facility, away from any significant weaving or high rates of lane change maneuvers. If there is a large range of  $v_{FP}$ , even across multiple lanes we suspect there will be moving bottlenecks forming voids ahead that violate the necessary stationary assumptions for LWR and SwA in the given lane. At moderate flows drivers will be able to escape slower leaders by moving to the faster lanes and in this region the qkFD should remain triangular. But under these conditions SwA will correctly predict that signals move with the vehicles and LWR does not apply. For the sake of this hypothetical example, assume the fastest lane (closest to the median) is numbered 1 and then the lane numbers increase towards the shoulder. Like Daganzo (2002), we suspect the drivers with faster  $v_{FP}$  will stay in lane 1 rather than slow down to fill a void in lane 2. As long as lane 1 is faster than lane 2, the hypothetical lane 1 should operate like the real lane 1 in this paper, while lane 2 will likely be far below its capacity and should continue to operate as if it were on a triangular qkFD since the drivers with higher  $v_{FP}$  can escape to the faster lane 1. As more vehicles migrate to lane 1 the lower end of  $v_{FP}$  in that lane will shift lower, and after enough vehicles have entered lane 1 the lower  $v_{FP}$  will pull  $v_1$  to the point where speeds are similar in the two fastest lanes. Even when the two fastest lanes come to this

<sup>&</sup>lt;sup>10</sup> If drivers also exhibit a range of jam spacing or reaction time (as per Newell, 2002) these congested regime parameters will probably just add noise to the traffic state measurements, but they should not on their own result in a concave qkFD in the absence of a range of  $v_{FP}$ .

equilibrium, as long as they remain in the free flow regime, the range of  $v_{FP}$  among the drivers should continue to yield moving bottlenecks behind voids in the individual lanes. These voids should still yield a concave qkFD and will continue to violate the stationary assumptions necessary to apply LWR and SwA. The voids should attract other vehicles to change lanes and enter the voids, but generally an entering vehicle will not have the same  $v_{FP}$  as the LHV behind the void. A vehicle that enters a void ahead of a driver with a lower  $v_{FP}$  will go faster than the moving bottleneck that gives rise to the void, and thus, the entering vehicle will simply trim the void on entry and then resume expanding the remaining void as they pull away from the slower vehicle that is the moving bottleneck without ever impacting its operation. Other vehicles will enter voids ahead of LHV that have a higher  $v_{FP}$ . When the entering vehicle has a lower  $v_{FP}$  then the moving bottleneck behind the void, the entering vehicle will effectively form a new void as their leader pulls away and the former moving bottleneck behind them will catch up, joining (or forming) a moving queue behind that even slower vehicle. As a moving queue in a given lane slows, it will increase the likelihood that one of the queued vehicles will want to overtake this moving queue by finding a void in the faster adjacent lane, and the cycle repeats. Voids pulling down q and blocking signals from propagating upstream in vehicle sequence should continue to disrupt lanes 1 and 2, yielding a concave qkFD while violating stationarity in such a way that inhibits LWR and SwA, similar the single lane process seen in this paper. Meanwhile, as the flow in the two fastest lanes increase, the speeds will drop until matching lane 3, and the process continues.

We suspect the subtle dynamics revealed in this research have gone unnoticed for so long because they are far below the resolution of conventional traffic monitoring. Hopefully this work will inspire others to examine their empirical data sets and join in the exploration for evidence to broadly support, limit the scope, or refute our findings herein. In the meantime, ongoing work by our group is showing that these general trends of LHV impacting the traffic state is not limited to HOV lane operations, our preliminary results show evidence of LHV pulling the state from a triangular qkFD to a smaller concave qkFD in general purpose lanes too. The results from general purpose lanes will be presented in a future paper.

This work likely has implications to other traffic flow models, if in no other way than to trigger an assessment to see if a given model is potentially sensitive to the dynamics presented herein. This assessment should consider at least three factors: (i) For traffic flow models that rely on the FD, one should check to make sure the moving bottlenecks and the associated voids that give rise to the reproducible concave qkFD will not disrupt the underlying assumptions of a given traffic flow model. (ii) Many traffic flow models assume there is a single characteristic signal propagating through each point in time and space (either within a single lane or across all lanes) this work shows that there is in fact a superposition of signals within a lane, e.g., Fig. 12i&o show separate signals moving concurrently both upstream and downstream in a single lane at the same location and at the same time. The superposition of signals and dependence on the adjacent lane necessitate greater complexity than provided by many traffic flow models. (iii) This work has also demonstrated that the underlying FD can potentially change shape so rapidly over time and space that one could not use the conventional approximation of a static FD curve to capture all of the dynamics. It might be very difficult to anticipate what shape the FD has at any instant or location, e.g., the underlying qkFD in a lane might differ from that of the same lane a few hundred ft away or the same location 30 sec later. Or from another perspective, the impacts of a rapidly changing FD might be another factor that contributes to the formation of disturbances or endurance of congestion, e.g., capacity drop.

Finally, this research has far reaching impacts on practice. Traffic flow theory is a critical input to many aspects of surface transportation, e.g., traffic management, traffic control, network design, vehicle routing, traveler information, and transportation planning all depend on models or simulation software that are based upon traffic flow theory. This empirical study has demonstrated significant deficiencies in conventional traffic flow models, which in turn, should degrade any application that relies on those models, be it traffic management or transportation planning. It will take time for the research community to characterize these newfound dynamics and incorporate them into the mainstream traffic flow models. In the meantime, these findings should lead to caution in accepting the predictions from traffic flow models and simulation software when the traffic exhibits a concave FD.

#### CRediT authorship contribution statement

**Benjamin Coifman:** Conceptualization, Methodology, Formal analysis, Investigation, Visualization, Supervision, Funding acquisition. **Balaji Ponnu:** Conceptualization, Methodology, Software, Formal analysis, Investigation, Visualization. **Paul El Asmar:** Validation, Investigation.

#### **Declaration of Competing Interest**

The authors declare that they have no known competing financial interests or personal relationships that could have appeared to influence the work reported in this paper.

#### Data availability

The data used are publicly available on our website

#### Acknowledgements

This material is based in part upon work supported in part by the National Science Foundation under Grant No. 1537423 and 2023857. The contents of this report reflect the views of the authors who are responsible for the facts and the accuracy of the data

presented herein. This report does not constitute a standard, specification or regulation.

#### References

```
Bertini, R.L., Boice, S., Bogenberger, K., 2006. Dynamics of Variable Speed Limit System Surrounding Bottleneck on German Autobahn. Transp. Res. Rec. 1978 (1), 149–159.
Braunstein, M.L., Laughery, K.R., 1964. Detection of vehicle velocity changes during expressway driving. Hum. Factors 6 (4), 327–331.
Breiman, L., Lawrence, R.L., 1973. Time scales, fluctuations and constant flow periods in uni-directional traffic. Transp. Res. 7 (1), 77–105.
Cassidy, M.J., 1998. Bivariate relations in nearly stationary highway traffic. Transp. Res. B 32 (1), 49–59.
Chen, D., Ahn, S., 2018. Capacity-drop at extended bottlenecks: Merge, diverge, and weave. Transp. Res. B Methodol. 108, 1–20.
```

Coifman, B., 2003a. Identifying the Onset of Congestion Rapidly with Existing Traffic Detectors. Transp. Res. A 37 (3), 277–291. Coifman, B., 2003b. Estimating Density and Lane Inflow on a Freeway Segment. Transp. Res. A 37 (8), 689–701.

Coifman, B., 2014a. Jam Occupancy and Other Lingering Problems with Empirical Fundamental Relationships. Transp. Res. Rec. 2422 (1), 104-112.

Coifman, B., 2014b. Revisiting the Empirical Fundamental Relationship. Transp. Res.- Part B 68, 173–184.

Coifman, B., 2015. Empirical Flow-Density and Speed-Spacing Relationships: Evidence of Vehicle Length Dependency. Transp. Res.- Part B 78, 54-65.

Coifman, B., Cassidy, M., 2002. Vehicle Reidentification and Travel Time Measurement on Congested Freeways. Transp. Res. A 36 (10), 899–917.

Coifman, B., Kim, S., 2011. Extended Bottlenecks, the Fundamental Relationship, and Capacity Drop on Freeways. Transp. Res.- Part A. 45 (9), 980-991.

Coifman, B., Ponnu, B., 2020. Adjacent Lane Dependencies Modulating Wave Velocity on Congested Freeways- An Empirical Study. Transp. Res. B 142, 84-99.

Coifman, B., Lyddy, D., Skabardonis, A., 2000. The Berkeley Highway Laboratory- Building on the I-880 Field Experiment, *Proc.* IEEE ITS Council Annual Meeting, IEEE, pp. 5–10.

Coifman, B., Wang, Y., 2005. Average Velocity of Waves Propagating Through Congested Freeway Traffic, Proc. of the 16th International Symposium on Transportation and Traffic Theory, July 19-21, 2005, College Park, MD, pp. 165-179.

Daganzo, C.F., 2002. A behavioral theory of multi-lane traffic flow. Part I: Long homogeneous freeway sections. Transp. Res. B 36 (2), 131–158.

Drake, J., Schofer, J., May, A., 1967. A Statistical Analysis of Speed Density Hypotheses, Highway Research Record. No. 154, 53–87.

Duckstein, L., Unwin, E.A., Boyd, E.T., 1970. Variable perception time in car following and its effect on model stability. IEEE Trans. Man-Machine Syst. 11 (3), 149–156.

Duret, A., Ahn, S., Buisson, C., 2012. Lane flow distribution on a three-lane freeway: General features and the effects of traffic controls. Transp. Res. Part C: Emerg. Technol. 24, 157–167.

Duret, A., Bouffier, J., Buisson, C., 2010. Onset of congestion from low-speed merging maneuvers within free-flow traffic stream: Analytical solution. Transp. Res. Rec. 2188 (1), 96–107.

Edie, L., Baverez, E., 1967. Generation and propagation of stop-start traffic waves. In: vehicular traffic science. *Proceedings of the Third International Symposium on the Theory of Traffic Flow.* Operations Research Society of America.

Greenshields, B., 1935. A Study of Traffic Capacity. Proc. of the Highway Research Board 14, 448-477.

Hall, F., Allen, B., Gunter, M., 1986. Empirical Analysis of Freeway Flow-Density Relationships. Transp. Res. A Policy Pract. 20 (3), 197-210.

Hall, F., Brilon, W., 1994. Comparison of Uncongested Speed-Flow Relationships Using Data from German Autobahns and North American Freeways. Transp. Res. Rec. 1457, 35–42.

Hall, F., Hurdle, V., Banks, J., 1992. Synthesis of Recent Work on The Nature of Speed-Flow and Flow-Occupancy (or Density) Relationships on Freeways. Transport. Res. Rec. No. 1365, 12–18.

Hurdle, V.F., Merlo, M.I., Robertson, D., 1997. Study of Speed-Flow Relationships on Individual Freeway Lanes. Transp. Res. Rec. 1591 (1), 7-13. Transp. Transp. Res. Rec. 1591 (1), 7-13. Transp. Trans

Hsu, P., Banks, J., 1993. Effects of Location on Congested-Regime Flow-Concentration Relationships for Freeways. Transport. Res. Rec. No 1398, 17–23.

Kesting, A., Treiber, M., Helbing, D., 2007. General Lane-Changing Model MOBIL for Car-Following Models. Transport. Res. Record, Transport Res. Board 1999, 86–94

Knoop, V., Daamen, W., 2017. Automatic fitting procedure for the fundamental diagram. Transportmetrica B: Transport Dynamics 5 (2), 129-144.

Laval, J., 2007. Linking synchronized flow and kinematic waves. In: *Traffic and Granular Flow* 05. Springer, Berlin, Heidelberg, pp. 521–526. Laval, J., 2009. Effects of geometric design on freeway capacity: Impacts of truck lane restrictions. Transp. Res. B Methodol. 43 (6), 720–728.

Leclercq, L., Chanut, S., Lesort, J.B., 2004. Moving bottlenecks in Lighthill-Whitham-Richards model: A unified theory. Transp. Res. Rec. 1883 (1), 3-13.

Leclercq, L., Knoop, V., Marczak, F., Hoogendoorn, S.P., 2016. Capacity drops at merges: New analytical investigations. Transp. Res. Part C: Emerging Technologies 62, 171–181.

Li, J., Zhang, H.M., 2011. Fundamental diagram of traffic flow: new identification scheme and further evidence from empirical data. Transp. Res. Rec. 2260 (1), 50–59.

Lighthill, M., Whitham, G., 1955. On Kinematic Waves II. a Theory of Traffic Flow on Long Crowded Roads. Proc. Royal Society of London Part A 229 (1178), 317–345.

Logghe, S., Immers, L.H., 2008. Multi-class kinematic wave theory of traffic flow. Transp. Res. B Methodol. 42 (6), 523-541.

Mortimer, R., 1971. The value of an accelerator release signal. Hum. Factors 13 (5), 481–486.

Munjal, P., Hsu, Y., Lawrence, R., 1971. Analysis and Validation of Lane-Drop Effects on Multi-Lane Freeways. Transp. Res. 5 (4), 257–266.

Munoz, J., Daganzo, C., 2002. Moving bottlenecks: A Theory Grounded on Experimental Observation, Proc. of the 15th International Symposium on Transportation and Traffic Theory (ISTTT15), pp. 441–461.

Newell, G., 1998. A moving bottleneck. Transp. Res. B Methodol. 32 (8), 531–537.

Newell, G.F., 2002. A simplified car-following theory: a lower order model. Transp. Res. B 36 (3), 195–205.

Ponnu, B., Coifman, B., 2015. Speed-Spacing Dependency on Relative Speed from the Adjacent Lane: New Insights for Car Following Models. Transp. Res.-Part B 82, 74–90

Ponnu, B., Coifman B., 2017. When adjacent lane dependencies dominate the uncongested regime of the fundamental relationship, *Transport. Res. Part B*, Vol. 104, pp. 602-609.

Punzo, V., Tripodi, A., 2007. Steady-State Solutions and Multiclass Calibration of Gipps Microscopic Traffic Flow Model. Transp. Res. Rec. 1999 (1), 104–114. Qian, Z.S., Li, J., Li, X., Zhang, M., Wang, H., 2017. Modeling heterogeneous traffic flow: A pragmatic approach. Transp. Res. B Methodol. 99, 183–204. Richards, P., 1956. Shock Waves on the Highway. Oper. Res. 4 (1), 42–51.

Rudjanakanoknad, J., 2012. Capacity change mechanism of a diverge bottleneck. Transp. Res. Rec. 2278 (1), 21-30.

Srivastava, A., Geroliminis, N., 2013. Empirical observations of capacity drop in freeway merges with ramp control and integration in a first-order model. Transport. Res. Part C: Emerging Technol. 30, 161–177.

Van Wageningen-Kessels, F., Van Lint, H., Hoogendoorn, S.P., Vuik, K., 2010. Lagrangian formulation of multiclass kinematic wave model. Transp. Res. Rec. 2188 (1), 29–36.

Wang, C., Coifman, B., 2008. The Effect of Lane-Change Maneuvers on a Simplified Car-following Theory. IEEE Trans. Intell. Transp. Syst. 9 (3), 523-535.

Wang, H., Ni, D., Chen, Q.Y., Li, J., 2013. Stochastic modeling of the equilibrium speed-density relationship. J. Adv. Transp. 47 (1), 126-150.

Wardrop, J., 1952. "Some Theoretical Aspects of Road Traffic Research", Proc. Inst. Civil Engineers, Part II 1, 325–362.

Xuan, Y., Coifman, B., 2012. Identifying Lane Change Maneuvers with Probe Vehicle Data and an Observed Asymmetry in Driver Accommodation. Journal of Transportation Engineering, ASCE 138 (8), 1051–1061.

Yang, D., Jin, J., Ran, B., Pu, Y., Yang, F., 2013. Modeling and Analysis of Car-Truck Heterogeneous Traffic Flow Based on Intelligent Driver Car-Following Model, Proc. of the Transportation Research Board 92nd Annual Meeting, 18p.

Zhang, H.M., 2002. A non-equilibrium traffic model devoid of gas-like behavior. Transp. Res. B Methodol. 36 (3), 275–290. Zhang, H.M., 2003. Anisotropic property revisited—does it hold in multi-lane traffic? Transp. Res. B Methodol. 37 (6), 561–577.